CFRP as Shear and End-Zone Reinforcement in Concrete Bridge Girders

Mitchell Drake Magee

Thesis submitted to the Faculty of the
Virginia Polytechnic Institute and State University
in partial fulfillment of the requirements for the degree of

Master of Science
In
Civil Engineering

Carin L. Roberts-Wollmann, Chair
Thomas E. Cousins
Cristopher D. Moen

May 2nd, 2016
Blacksburg, VA

Keywords: NEFMAC, CFRP, Shear, Transverse Reinforcement, Concrete Bridge Girders

CFRP as Shear and End-Zone Reinforcement in Concrete Bridge Girders

Mitchell Drake Magee

Abstract

Corrosion of reinforcing steel is a major cause of damage to bridges in the United States. A possible solution to the corrosion issue is carbon fiber reinforced polymer (CFRP) material. CFRP material has been implemented as flexural reinforcement in many cases, but not as transverse reinforcing. The CFRP material studied in this thesis was new fiber composite material for reinforcing concrete (NEFMAC) grid, which consists of vertical and horizontal CFRP tows that form an 8 in. by 10 in. grid. The use of NEFMAC grid as transverse reinforcing has not been previously investigated.

First, the development length of NEFMAC grid was determined. Next, an 18 ft long 19 in. deep beam, modeled after prestressed Bulb-T beams, was created with NEFMAC grid reinforcement. The beam was loaded with a single point load near the support to induce shear failure. Beams were fitted with instrumentation to capture shear cracking data. Shear capacity calculations following four methods were compared to test results. Lastly, a parametric study with strut-and-tie modeling was performed on Precast Bulb-T (PCBT) girders to determine the amount of CFRP grid needed for reinforcement in the end zone.

This thesis concludes that NEFMAC grid is a viable shear design option and presents the initial recommendations for design methods. These methods provide a basis for the design of NEFMAC grid shear reinforcing that can be used as a starting point for future testing. For design, the full manufacturer's guaranteed strength of NEFMAC grid should be used as it is the average reduced by three standard deviations. AASHTO modified compression field theory provides the best prediction of shear capacity. For end zone design, working stress limits for CFRP grids need to be increased to allow more of the strength to be implemented in design.

CFRP as Shear and End-Zone Reinforcement in Concrete Bridge Girders

Mitchell Drake Magee

Abstract - Public

A major concern with concrete bridge girders in the United States is corrosion of the reinforcing steel. This corrosion causes costly repairs and replacements, creating a need for corrosive resistant design alternative. One alternative comes from the use of carbon fiber reinforced polymer (CFRP) materials. CFRP materials do not corrode when exposed to corrosive agents like steel, providing a good alternative for designs. This thesis studies the use of new fiber composite material for reinforcing concrete (NEFMAC) grid as shear reinforcement in bridge girders, as well as the use of CFRP grids as end zone reinforcement.

The NEFMAC grid was used as shear reinforcement in a small-scale concrete bridge beam. The beam was reinforced with two different amounts of NEFMAC grid on each side to allow for two tests. The testing with NEFMAC grid was compared to identical tests performed with steel and other CFRP materials. Results showed that NEFMAC grid performed well compare to the other reinforcement, and that current design methods are too conservative when CFRP materials are used.

The end-zone of a beam is an area susceptible to cracking during the initial stages of the beam's life-span. This cracking is an area of concern due to the ability of corrosive agents easily get to the reinforcing steel. Analyses and modeling of this region was performed on full-scale bridge beams. Through this analysis, it was determined that CFRP grids are not a viable source of reinforcement in the end-zone region due to strict current design limits set on the material.

Acknowledgements

I would like to thank the following people:

- Dr. Carin Roberts-Wollmann for advising me throughout the project and always making time to answer my questions, even the simple ones.
- Dr. Tommy Cousins and Dr. Cris Moen for participating in my advisory committee and providing helpful insight throughout the process.
- Brett Farmer and Dennis Huffman for all their help in the laboratory. Without their guidance many graduate students would be lost out in the lab.
- Dr. David Mokarem for his help in experimentation at the lab and general sports talk – Go Hokies!
- John Ward for his guidance during his last semester and easing my transition into the project.
- Carrie Field for her support during the semester with testing and awesome music selection in the office.
- VCTIR and CAIT at Rutgers for providing the funding to make this research and thesis possible.
- My fiancé, Tara Rodriguez, who has kept me planted during this entire process. You were my rock when the path was tough. I look forward to starting our lives together.
- My Parents – without them I would never have had this opportunity. I owe it all to them for who I am today.
- My peers in CEE SEM for general encouragement throughout the project and grad school.

Contents

List of Figures

List of Tables:

1 - Introduction

A major concern in designing prestressed and reinforced concrete structures is the effect that corrosive agents have on the reinforcing steel. In coastal regions such as Hampton Roads and Newport News in Virginia, this issue is accelerated. Corrosive chlorides in seawater deteriorate the steel reinforcing, causing many of the prestressed concrete bridges to age prematurely. This aging leads to repairs that are both costly and time consuming. In order to stop this corrosive issue in future bridges, design alternatives need to be researched.

1.1 – Carbon Fiber Reinforced Polymers

Carbon fiber reinforced polymer (CFRP) is a material that can be used as an alternative to reinforcing steel. The use of CFRP has quickly gained footing in the United States as a replacement for reinforcement steel due to its corrosion resistance. A beneficial factor of using CFRP as shear reinforcing is the corrosion resistance causing an increase in design life. However, has a brittle failure mode in tension as opposed to the ductile failure of reinforcing steel. Virginia Department of Transportation (VDOT) is interested in implementing CFRP into designs due to its corrosion resistance.

For the VDOT project, CFRP grids were investigated as alternatives for shear and end zone reinforcement. To ensure safe design with CFRP grids, testing needed to be conducted to determine their performance as shear reinforcement. First, this was done by determining the development length of the CFRP grid. Then the grids were tested as shear reinforcement for scaled down versions of Bulb-T beams. The results for these tests were then compared to a few current methods for determining shear capacity. The first grid used was NEFMAC grid, which is produced in Japan. This grid comes in 9 ft by 6 ft sheets, and can easily be cut and spliced as needed for design. The second grid used was C-grid, which is a lighter alternative to NEFMAC

grid. C-grid is produced in the United States making it easier to obtain than NEFMAC grid. Both of these grids are easy to cut on site and can be used in different configurations. NEFMAC grid is shown in Figure 1, C-grid is shown in Figure 2. Shear testing for C-grid was completed by Ward (2016), and shear testing for NEFMAC grid is presented in this thesis.

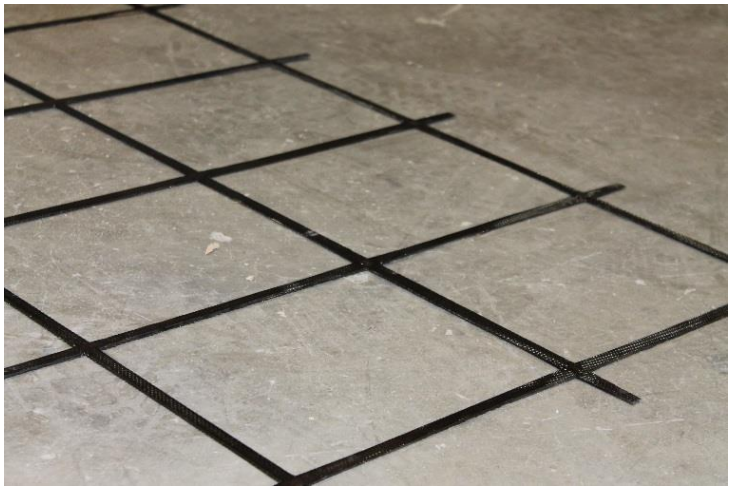

Figure 1: NEFMAC Grid Material

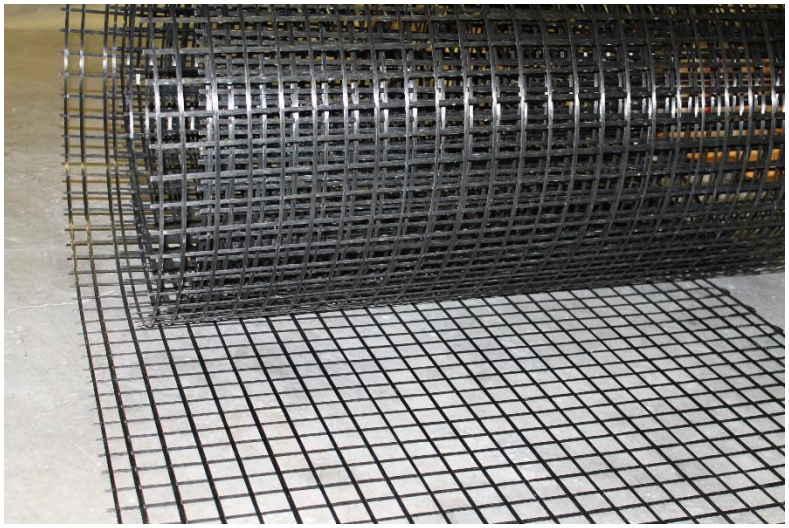

Figure 2: C-Grid Material

1.2 – Anchorage Zone Cracking

An anchorage zone is the region in prestressed concrete members where the force from the prestressed steel is transferred to the concrete. These forces are gradually transferred by bond between concrete and steel. Compressive stresses are formed through this transfer and spread through the member in a curved pattern until a linear stress distribution occurs. These curved compressive stresses create tensile stresses that can cause cracking in the member. A typical anchorage zone crack pattern for anchorage zones of precast Bulb-T (PCBT) beams is shown in Figure 3.

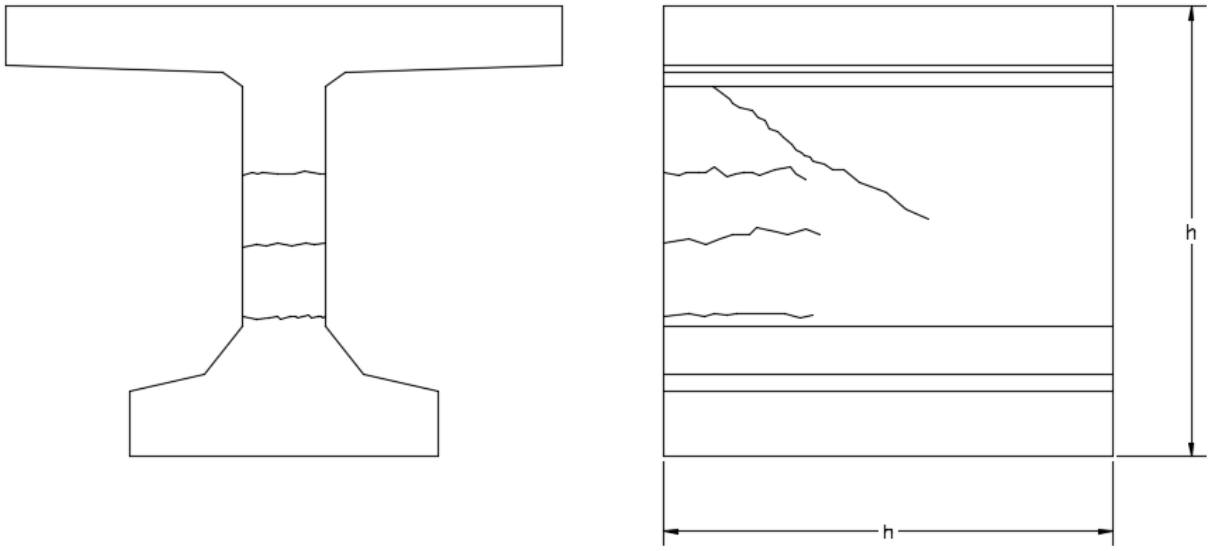

Figure 3: Typical Anchorage Zone Crack Pattern for PCBT

`

Anchorage zone cracking causes concern in design due to allowing corrosive agents to reach the reinforcing. Repairs can be made to these cracks, however, they are expensive and time consuming. In order for VDOT to implement CFRP reinforcing in girders, the proper amount of end zone CFRP reinforcement to prevent cracking must be determined.

1.3 – Project Objective

The first objective of the project was to determine the development length of NEFMAC grid. The second objective was to investigate the behavior and strength of concrete beams containing NEFMAC grid transverse reinforcement. To accomplish the second objective, comparisons were made with findings from Ward (2016) from testing C-grid and steel reinforced beams. The tests were designed to induce a shear failure of the beams.

The third objective of the project was to determine the suitability of using shear design methodologies given by ACI (2012, 2006, & 2004) and AASHTO (2012) to determine the shear strength of a beam reinforced with NEFMAC grid. The beam tests in this project with NEFMAC grid reinforcement were compared to the tests performed by Ward (2016). This comparison showed any differences in crack control and shear strength between the reinforcing material.

The fourth objective was to evaluate anchorage zone cracking and determine if CFRP grid is a viable option for reinforcement in this region. The final objective is to provide recommendations for the design of beams using NEFMAC grid transverse reinforcement for shear strength. These recommendations are presented at the end of this thesis.

1.4 – Scope of Project

1.4.1 – NEFMAC grid Development Tests

NEFMAC grids were tested to examine their development lengths. These tests were conducted with embedment lengths of the NEFMAC grid into concrete of 4, 6, and 8 in. These tests were conducted for recommended development length in future designs.

1.4.2 – Beam Tests

One beam 18 in. deep and 18 ft long was fabricated to test the NEFMAC grid as shear reinforcing. The beam had the minimum shear reinforcement ratio as per AASHTO LRFD in one half and typical shear reinforcement ratio in the other half. The beam was designed to have similar strength to that found in Ward's (2016) test specimens as determined by AASHTO LRFD code provisions. Beams were designed to have shear failures during testing.

1.4.3 – Parametric Study

A parametric study was performed on the three most commonly used prestressed PCBT girder cross sections. The three cross sections were tested with different span lengths and beam spacing, resulting in nine different cases. This was done to evaluate the feasibility of using CFRP grids as transverse reinforcing in anchorage zones of prestressed concrete girders. The study used strut-and-tie modeling to determine required shear capacities for the transverse reinforcing. The study was performed twice, once only using CFRP grid for the shear reinforcement, and a second time using a combination of steel stirrups and CFRP grid for the shear reinforcement.

2 – Literature Review

2.1 – CFRP as Reinforcing/Prestressing

CFRP has great potential to be used as reinforcing and prestressing in concrete. However, CFRP is a very brittle material compared to steel. Typical prestressing strands yield at 1% elongation, but do not fail until 4-5% elongation (Nilson, 1987). A CFRP prestressing rope exhibit about 1.7% elongation before failure and is linear elastic until fracture (Grace, Ushijima,

Baah, & Bebway, 2013). Compared to steel, CFRP is a very brittle material, which can create design concerns.

2.1.1 – CFRP as Flexural Reinforcing

Grace has completed a number of research projects using CFRP prestressing strand, providing a good initial starting point for this research and considering the use of CFRP strands in the design of prestressed concrete. For example, Grace presents a design process using CFRP prestressing strands in multiple levels in a beam (Grace & Singh, 2003). Due to CFRP's corrosion resistance, Department of Transportations (DOTs) are starting to consider CFRP in prestressed concrete to increase the design life (Grace et al., 2012).

Grace has developed a method for design of prestressed concrete beams containing CFRP flexural reinforcement. This design is done by calculating the balanced reinforcement ratio, the amount of reinforcing which results in concrete crushing and the rupture of the bottom layer of CFRP tendons occurring simultaneously (Grace & Singh, 2003). Using this reinforcing ratio, the beam's nominal strength is determined. This method utilizes a strain compatibility approach with the ultimate compressive strain of concrete taken as 0.003. In a parametric study, as the prestressing level and reinforcement ratio of the beams were increased, the beams showed more strength and ductility (Grace & Singh, 2003).

It is important to note the differences between steel prestressing and CFRP prestressing. A key note from this research is that as the CFRP beam is reinforced with a larger amount of reinforcement, the beam increases ductility. CFRP has a brittle rupture failure that does not undergo a large elongation like steel. This is an aspect of design that engineers need to take into account since it is the opposite of the traditional steel reinforcing used currently.

To correlate the findings, Grace tested an AASHTO Bulb-T beam system that was reinforced and prestressed with CFRP. He found that his design method's predicted strength was comparable to the actual tested strength and the system maintained its structural integrity under normal service loads (Grace et al., 2013). These findings show that bridge beams can be safely designed with CFRP prestressing if the design is used correctly. To maintain safety with CFRP, designers need to account for its brittle behavior and ensure the actual failure strength is much higher than the CFRP strength used in calculations (Grace & Singh, 2003).

2.2 – CFRP Shear Reinforcing

CFRP has been implemented in design for flexural reinforcing, however, its use as other types of reinforcing have not been studied extensively (Grace et al, 2012). Due to its corrosion resistance, VDOT is interested in the use of CFRP reinforcing for shear reinforcement. Shear reinforcing tends to have the most exposure to corrosion since the reinforcing has less cover than other reinforcement in the beam. With shear reinforcing, spalling of the concrete occurs when corrosive chlorides react with the typical steel stirrups. In order to increase the life span of bridges, CFRP can be used as shear reinforcing to mitigate corrosion damage.

For prestressed design, shear capacity is influenced by transverse reinforcement, concrete properties, and harped or draped prestressing cable. For CFRP prestressing, the strands are typically straight due to the difficulty and danger of draping or harping CFRP strands. For these reasons, CFRP prestressing is usually straight strands, which do not have an added benefit for shear design. Similar to straight-strand prestressing, longitudinal reinforcement does not increase shear resistance in the reinforced section.

One deterrent for the use of CFRP as reinforcing is the cost of the material. However, using CFRP as transverse reinforcing can reduce rehabilitation costs of structures and increase

the overall life-span for the bridge. Also, as design with CFRP becomes more wide spread, more options of CFRP products will become available which may decrease costs through competition. This may enable CFRP to become as cost effective as steel reinforcing for transverse reinforcing—especially when accounting for overall maintenance and rehabilitation costs of the structures.

2.2.1 – NEFMAC Grid

NEFMAC grid is a CFRP product that is produced outside of the United states and is used as a replacement for welded wire mesh. NEFMAC grid comes in different member thicknesses and spacing configurations which can be altered depending on the application. NEFMAC was used by one company in Canada in different applications such as reinforcing in a bridge deck (Steffen et al., 2003). Constructability with NEFMAC was faster compared to steel reinforcing due to the ability to lay large grid sheets at once and tying them in place at fewer locations. The weight of NEFMAC allowed large sheets to be placed by fewer people when compared to welded wire mesh (Steffen et al., 2003). However, due to the light weight of the grid, an issue that was noticed was it would float when concrete was placed. This issue was resolved by tying down the grid to PVC spacers (Steffen et al., 2003).

2.2.2 – C-Grid

Similar to NEFMAC grid, C-Grid is CFRP product that can be used in place of welded wire mesh. C-Grid is readily available in the United States since it is produced by Chomarat North America in Anderson, SC. C-Grid is one of the only CFRP concrete reinforcing manufacturers in the US. C-Grid was initially designed for use in precast wall panels, but has also been implemented in the top flange of precast double T's (Ward, 2016). Compared to typical steel, C-Grid requires less cover, which has resulted in the ability to use thinner flanges in

Double T's (Ward, 2016). The tension capacity of C-Grid is on the order of 5 kip/ft width of material. Since this capacity is weaker than steel stirrups, C-Grid has not been implemented as shear reinforcement for large scale members. If C-Grid gains popularity in the design market, it is possible that Chomarat could start producing a higher strength material (Ward, 2016).

2.3 – Methods for Shear Design with CFRP

2.3.1 – AASHTO Shear Design Method

Specifications for prestressed and reinforced concrete member design for use in bridges is provide by The American Association of State Highway and Transportation Officials (AASHTO) LRFD Bridge Design Specifications. These specifications are for use with steel reinforcing and prestressing. The AASHTO shear resistance is presented in chapter 5 of the specifications in three parts: resistance of the concrete, resistance from transverse reinforcement, and the additional resistance from the vertical prestressing forces. There are several methods, but this thesis will present the general shear design method given in section 5.

The shear resistance of a reinforced beam found using the General Method is based upon the Modified Compression Field Theory (MCFT), developed by Vecchio & Collins (1986). The concrete shear resistance equation is shown below as Equation 1.

$$V_c = 0.0316\beta\sqrt{f'_c}\,b_v d_v \quad (kips) \qquad \text{(Eq 1)}$$

Where:

β = Cracked concrete ability to transmit tension and shear factor

f'_c = 28 day compressive strength of concrete (ksi)

b_v = Effective web width (in.)

d_v = Effective shear depth (in.)

The shear resistance from the transverse reinforcement is given based on the Equation 2 given below.

$$V_s = \frac{A_v f_y d_v (cot\theta + cot\alpha) sin\alpha}{s} \quad (kips) \qquad \text{(Eq 2)}$$

Where:

s = Spacing of transverse ties/tows (in.)

A_v = Area of transverse reinforcement between each spacing (in.^{2})

α = Angle of transverse from horizontal reinforcement (degrees)

θ = Angle of diagonal compressive stresses (degrees)

f_y = Specified yield strength of transverse reinforcing (ksi)

The value of f_y must be equal to or less than 0.0035 times the modulus of elasticity for the transverse reinforcing. Equation 2 can be simplified when the transverse reinforcing is designed at 90 degrees to the longitudinal axis, as seen in Equation 3 below.

$$V_s = \frac{A_v f_y d_v cot\theta}{s} \quad (kips) \qquad \text{(Eq 3)}$$

Since transverse reinforcing is usually perpendicular with the longitudinal reinforcing, Equation 3 is one of the most common equations used in design. θ is dependent upon the strain in the tension steel, as seen below in Equation 5.

For prestressed sections, additional shear resistance, V_p, is obtained from the harped or draped strands. However, the experimental testing in this thesis does not include prestressed sections, so it will be excluded from calculations.

The equations for β and θ from the AASHTO general method in chapter 5 are presented in Equations 4 and 5. To account for concrete strength, the factor β (ability of diagonally cracked concrete to transmit tension and shear forces) is used. The equation for calculating β is

found below in Equation 4. Concrete strength is based on the capacity pre-cracking and post cracking. Transverse and longitudinal reinforcement is used to interlock the post cracking aggregates to maintain the concrete capacity for shear resistance.

$$\beta = \frac{4.8}{(1 + 750\epsilon_s)} \quad \text{(Eq 4)}$$

$$\theta = 29 + 3500\varepsilon_s \quad \text{(Eq 5)}$$

Where:

ε_s = Strain in tension reinforcement

As the strain in tension reinforcement, ε_s, is decreased, β increases and θ decreases. Based on this correlation and Equations 1 and 3 above, as ε_s decreases, the shear resistance of the transverse reinforcement will increase. This leads to the fact that at a constant loading, increasing the flexural reinforcement will reduce the strain in this reinforcing and increase the shear resistance of the transverse reinforcement.

The calculation of ε_s by AASHTO is provided in equation 6 below.

$$\epsilon_s = \frac{\frac{[M_u]}{d_v} + 0.5N_u + [V_u - V_p] - A_{ps}f_{po}}{E_sA_s + E_pA_{ps}} \quad \text{(Eq 6)}$$

Where:

M_u = Factored moment (kip-in.)

N_u = Factored axial load (kip)

V_u = Factored shear force (kip)

V_p = Shear resisting component of prestressing (kip)

E_s = Modulus of elasticity of reinforcing steel (ksi)

A_s = Area of reinforcing steel (in^2)

E_p = Modulus of elasticity of prestressing steel (ksi)

A_{ps} = Area of prestressing streel (in^2)

f_{po} = Parameter to account for amount of force in prestressing cables (ksi), usually taken as $0.7f_{pu}$

f_{pu} = Ultimate stress in prestressing steel (ksi)

If the value of ϵ_s is negative, it should be taken as zero.

The minimum amount of transverse reinforcement provided by AASHTO is shown in Equation 7.

$$A_v \geq 0.0316\sqrt{f'_c}\frac{b_v s}{f_y} \quad \text{(Eq 7)}$$

Where:

A_v = Area of a transverse reinforcement within distance s ($in.^2$)

The AASHTO general method is commonly used by bridge engineers. It is an easy approach to follow to calculate shear resistance in reinforced and prestressed concrete designs.

2.3.2 – ACI 318-14 Shear Design Method

The American Concrete Institute (ACI) 318 Building Code provides a method for shear capacity in reinforced beams with steel. ACI's shear capacity designs for prestressed beams will be omitted from this thesis due to the experimental portion only including reinforced beams. ACI provides the nominal shear resistance through the summation of two components—shear resistance of the concrete and reinforcing steel.

Equation 22.5.5.1 is the most commonly used equation in ACI 318-14 for the design of the contribution of concrete strength in shear in flexural members. This equation is provided below in Equation 8.

$$V_c = 2\lambda\sqrt{f'_c}b_w d \quad (lbs) \tag{Eq 8}$$

Where:

λ = modification factor the tensile and shear strength of lightweight concrete (1.0 if normal weight concrete)

f'_c = 28-day compressive strength of concrete (psi)

b_w = Minimum web width (in.)

d = Depth of section from extreme compression fiber to center of tension reinforcement (in.)

The contribution of steel is expressed in equation 22.5.10.5.3 which is presented below as Equation 9.

$$V_s = \frac{A_v f_{yt} d}{s} \quad (lbs) \tag{Eq 9}$$

Where:

s = center-to-center spacing of transverse reinforcement (in.)

A_v = Area of transverse reinforcement within the spacing (in.^{2})

f_{yt} = Specified yield strength of transverse reinforcement (psi)

CFRP does not yield, so f_{yt} should be taken as the design strength of the bar or tow being used for calculations. For this design method, f_{yt} must be less than or equal to 80 ksi.

2.3.3 – ACI 440.4R-04 Shear Design Method

ACI 440.4R-04 proposes guidelines for the design of prestressed FRP concrete sections. This guideline gives a method for designing prestressed concrete sections with FRP as prestressing tendons and additional shear reinforcement. ACI 440.4R.04 and ACI 318 use a shear design method that is almost identical. Equations 5-2 and 5-3 from ACI 440.4R.04 are

shown below as Equations 10 and 11 respectively. This method does not include a contribution to shear resistance from prestressing. This is most likely due to FRP prestressing primarily being straight-strand prestressing. Harped or draped prestressing are the portions of prestressing that increase shear resistance to concrete sections.

$$V_c = 2\sqrt{f'_c}b_w d \quad (lbs) \tag{Eq 10}$$

$$V_{frp} = \frac{A_v f_{fb} d}{s} \quad (lbs) \tag{Eq 11}$$

Where:

f_{fb} = Strength of bent portion of FRP bar (psi)

The term, f_{fb}, is calculated using Equation 12 below. This calculation depends on the value of ϕ_{bend}, which is calculated using Equation 13. The bent portion of FRP bars tend to be the weakest portion of the bar, therefore, these calculations conservatively account for the different combinations of bar diameter and bend radii in determining f_{fb}. Bent FRP stirrups should have 90-degree bends, and should have a $\frac{r}{d_b}$ of 3.0 or greater with a minimum tail length of $12d_b$.

$$f_{fb} = Lesser\ of: \phi_{bend} f_{fu}\ or\ 0.002E_f \tag{Eq 12}$$

$$\phi_{bend} = \left(0.11 + 0.05\frac{r}{d_b}\right)\ and\ 0.25 \leq \phi_{bend} \leq 1.0 \tag{Eq 13}$$

Where:

f_{fu} = Design tensile strength of FRP (psi)

E_f = Design modulus of elasticity of FRP (psi)

ϕ_{bend} = Strength reduction factor

r = Radius of bend (in.)

2.3.4 – ACI 440.1R-06 Shear Design Method

ACI 440.1R-06 provides guidelines for the use of FRP reinforcement in reinforced concrete sections. This shear capacity method uses the summation of the concrete and transverse reinforcement shear resistance equations. The concrete resistance equation is different than the other two ACI methods shown because it ignores aggregate interlocking. For this method, the assumption is made that all of the concrete contribution to shear strength is from the uncracked concrete above the neutral axis. The concrete contribution to shear resistance from ACI 440.1R is shown in Equation 14.

$$V_c = 5\sqrt{f'_c}b_w c \quad (lbs) \tag{Eq 14}$$

Where:

c = distance to neutral axis from the compression face (in.)

This equation was developed to provide a better estimate of concrete contribution to shear strength based on the strain in the longitudinal steel in the section. The neutral axis is calculated using the cracked transformed section which uses the stiffness of the longitudinal reinforcement. As the stiffness of the longitudinal reinforcement increases, c will increase. As c increases, the amount of the section in compression is increased, which can reduce cracking and increase shear resistance.

However, for the testing in this thesis the sections have large flanges, raising the neutral axis out of the web of the beam. Therefore, the shear funnel approach was used to determine the concrete's shear resistance (Tureyen et al., 2006). This method accounted for the uncracked concrete's contribution to shear strength, but only for concrete close to the web. However,

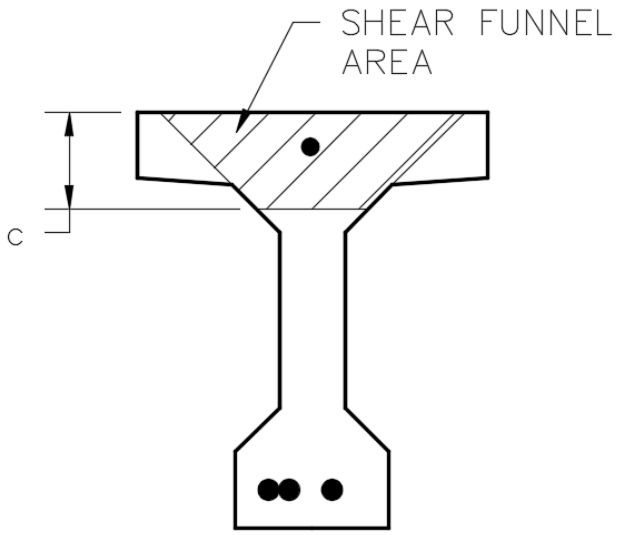

Figure 4: Shear Funnel Diagram for Beam Specimen

instead of using the suggested 45° angle, the angle of the taper was used. Figure 4 provides a diagram of the shear area used in the calculations. The area of the shear funnel replaces the $b_w c$ term in Equation 14.

The reinforcing shear resistance is very similar to the other ACI methods that have been previously described. The FRP resistance equation is shown as Equation 15.

$$V_f = \frac{A_{fv} f_{fv} d}{s} \quad (lbs) \qquad \text{(Eq 15)}$$

Where:

A_{fv} = area of transverse FRP reinforcement within spacing, s (in^2)

f_{fv} = Design tensile strength of FRP (psi)

The term f_{fv} must be equal to or less than the smallest of: design tensile strength of bar, design bend strength of bar, or 0.004 times the modulus of elasticity of the FRP bar.

2.4 – Prior FRP Shear Tests

2.4.1 – Fam – 1996

Fam (1996) tested six large scale simply supported I-beams (five were reinforced with CFRP prestressing and transverse reinforcing, and one with steel prestressing and transverse reinforcing). For the CFRP reinforced beams, the prestressing varied in size and type and the transverse reinforcing varied in spacing and type. Transverse reinforcement included carbon fiber composite cable (CFCC) stirrups, CFRP Leadline stirrups and steel stirrups in the control beam.

Based on the results, the modified compression theory correlated the best with the shear behavior in the beam. This study found that reinforcing with CFRP provided similar results to steel reinforcement. However, the failures were sudden and brittle when shear failure occurred. Once the CFRP transverse reinforcing failed, all of the load shifted to the longitudinal reinforcing causing it to fail. This type of failure is important to understand to ensure safe designs with CFRP material.

2.4.2 – Shehata, Morphy, and Rizkalla - 1997

Shehata, Morphy, and Rizkalla performed tests using CFCC stirrups as transverse reinforcement (1997). The stirrups that were tested are CFCC stirrups, CFRP Leadline stirrups, and glass fiber reinforced polymer (GFRP) C-Bar stirrups.

Development length testing was performed initially on the fiber reinforced polymer (FRP) strirrups. The findings were that for embedment lengths less than 6 in. before bend in bar, the bend would fail prematurely. This failure occurred as low as 43% of the straight bar strength. When the embedment depths were larger than 6 in., the stirrups developed full strength.

For the beam tests, six specimens were tested: three with CFRP Leadline stirrups, one with GFRP C-Bar stirrups, one with traditional steel stirrups, and one without transverse reinforcement. The findings of these tests were that the FRP specimens performed similar to the steel reinforced specimen. The CFRP Leadline stirrups were able to maintain similar crack widths to traditional steel transverse reinforcement. Due to the reduction in strength at the bends, it was noted that cracks were likely to cross the bent portions of the CFCC stirrups, and that design with these stirrups should be limited to 50% of their straight bar strength.

2.4.3 – Jeong, Lee, Kim, Ok, and Yoon – 2006

Jeong, Lee, Kim, Ok, and Yoon (2006) performed testing that used CFRP grids as transverse reinforcement. Prior to this study, the use of CFRP grids as transverse reinforcement has not been studied in depth. Jeong, Lee, Kim, Ok, and Yoon used the grid perpendicular to the length of the beam. This provided a stirrup-like set-up instead of using the grid as continuous longitudinal reinforcement.

Initially, tension testing was performed on the GFRP and CFRP materials. The findings were compared to the manufacturers provided properties, tensile strength was higher. From these findings, the authors believed that the manufacturer's provided properties could be used conservatively in design.

Four beam specimens were tested using GFRP bars as flexural reinforcement, and CFRP grid as shear reinforcement. The perpendicular CFRP grids were spaced longitudinally at 5 in., 7 in., 10 in., and 20 in. spacings. Beams were designed which used bundled GFRP longitudinal bars for the flexural reinforcement. To obtain large shear forces, the specimens were placed in four point bending with two point loads applied close to one support. The findings of these tests were that the larger the spacing of the shear reinforcement, the greater likelihood of shear failure.

The designs of these tests were completed using ACI 440.1-R, and the findings were similar to the expected failures when designed using these guidelines.

2.4.4 – Nabipaylashgari – 2012

Eight T-beams reinforced with CFRP prestressing were designed and tested by Nabipaylashgari (2012). Four of the beams had GFRP transverse reinforcement while the other four beams did not have transverse reinforcement. Three beams of each type of transverse reinforcing were placed under four-point bending with span to depth ratios of 1.5, 2.5, and 3.5. The last beam from each type of transverse reinforcing was placed under uniform loading.

All of the beams were tested under four-point bending led to shear failures. For 2.5 and 3.5 span to depth ratios, there was an 8% increase in shear resistance from the beams without transverse reinforcing to the beams with GFRP transverse reinforcing. For the last two beams tested with uniform loading, there was a 42% increase in shear cracking load and a 63% increase in nominal shear strength when the GFRP transverse reinforcing was included.

2.4.5 – Grace, Rout, Ushijima, and Bebway - 2015

Grace, Rout, Ushijima, and Bebway (2015) completed research into the use of CFCC stirrups for shear reinforcement in bridge girders. The first part of testing was to determine bend strength of the CFCC stirrups at a small scale. Findings indicated that when the embedment length was insufficient, the CFCC stirrups would slip before failure. When the embedment depth was sufficient, failure of the CFCC stirrups would occur just before the bend. Additional findings also showed that the maximum strain limitations of stirrups given in AASHTO as 0.35%, ACI 440.4R as 0.2%, and ACI 440.1R as 0.4% are conservative.

The second part of this study consisted of testing eleven full scale simple span prestressed beams. Nine of the beams were 39 ft long and two were 40 ft long. The transverse

reinforcement consisted of CFCC stirrups on one end and steel stirrups on the other end for each beam. Stirrup spacing was 4 in., 6in., and 8 in. for all the beam specimens. This testing found that at failure, the bends of the stirrups had a higher strain than the strain of the straight portion. Also, the findings show that the ACI 440.4 method for determining shear resistance is quite conservative. The authors recommend that to create a more accurate CFRP design, ACI 440.4 needs to be revised.

2.4.6 – Ward – 2016

Ward (2016) performed testing on four miniature Bulb-T beams that used CFRP as transverse reinforcement. The beams were designed with different materials as the transverse reinforcement. One beam was designed with steel stirrups, one beam was designed with CFCC stirrups, and two beams were designed with C-grid. Two different reinforcement ratios were used on each beam, resulting in eight beam designs and tests. The purpose of this testing was to create shear failures in the beams, and compare the failure loads to existing shear design methods previously presented in this section. Ward determined that C-grid could be utilized in shear design, however, current stress limitations for the reinforcement cause the designs to be overly conservative. By utilizing the full strength of C-grid in the design, the current design methods economically predicted shear failure. The results for C-grid presented by Ward (2016) were utilized in this thesis for comparison with NEFMAC grid.

2.5 – Anchorage Zone Design

As prestressed concrete became more prominent in the United States, issues with horizontal cracks forming at the beam ends immediately after prestress transfer became a design concern. These cracks allow corrosive agents to reach the steel reinforcing, causing internal damage to the beam. This damage is both time consuming and costly to repair. As a result,

different methods have been implemented for predicting and controlling these anchorage zone cracks.

2.5.1 – Current AASHTO Provisions

AASHTO LRFD Bridge Design Specifications (AASHTO, 2012) specifies the design of anchorage zone in pretensioned concrete girders. Article 5.10.10.1 specifies that the vertical reinforcement within 25 percent of the height of the member from the beam end must be able to resist at least 4 percent of the total prestressing force at transfer. The total working stress in the steel must be less than or equal to 20 ksi. The vertical reinforcement must be placed as close to the end of the beam as possible.

2.5.2 – Analytical Methods

2.5.2.1 – Gergely and Sozen Cracked Beam Model

Gergely and Sozen created a method to analyze anchorage zone cracks. The Gergely and Sozen method was used to design transverse reinforcement that would restrain this cracking. This method proposed a way to estimate the position of the first crack. The Gergely and Sozen method is based on equilibrium conditions of a cracked anchorage zone, and assumes that there will be horizontal cracking at the end region of a prestressed member.

Using bond-slip relationships, Gergely and Sozen created a method to control crack widths. In equation 16, Gergely and Sozen present the limit on stress in stirrups to obtain a desired crack width.

$$f_s = \sqrt{\frac{4E\sqrt{f'_c}w}{A}} \qquad \text{(Eq 16)}$$

Where:

f_s = Stress in the stirrups (psi)

E = Modulus of elasticity of stirrup (psi)

f'_c = Concrete compressive strength at transfer (psi)

A = Area of steel of one stirrup (in^2)

w = Desired crack width (in)

The designer can design the stirrup stress based on the desired crack width, and then compare the stress to the maximum allowable stress. Using the lower of these two stresses, the area of reinforcement required can be determined. This is done by dividing the minimum of the two stresses by a calculated tension force at the horizontal crack.

2.5.3 – Finite Element Model

2.5.3.1 – General

Finite element models (FEM) can provide insightful information on the prestressed forces into beam ends. However, when it comes to typical design, using finite element models can be tedious. In order to obtain accurate results, a non-linear analysis should be done to account for concrete cracking. Since the anchorage zone design of a pretensioned beam is a fairly small portion of the overall beam design, using the resources and time to run a non-linear analysis would not be warranted in the design industry.

2.5.4 – Strut-and-Tie Modeling

2.5.4.1 – General

Another way to analyze prestressed beam ends is with strut-and-tie models (STM). The end region of a beam is referred to as a disturbed zone, or D-region. A STM is a truss model of the D-region. This model is made of up compression members (struts) and tension members (ties) connected at nodes. The compressive forces are carried by concrete struts and the tensile forces are carried by reinforcing in the concrete. The length of the D-region for a pretensioned

beam is equal to the total depth of the member. Outside of this region, the assumptions for beam theory, that the stress distribution is linear and plane sections remain plane, apply.

Designers are able to pick the layout of the truss model for strut-and-tie modeling. However, different layouts could yield different results. To reduce these differences, the layout should follow the flow of elastic force through a section. Designers need to account for the flow of forces through a cracked section to ensure safe design and proper placement of reinforcement. The model does not have to satisfy compatibility but must remain in equilibrium between the applied loads and reactions. Limits are placed on the stress in the steel to reduce crack widths.

2.5.4.2 – Castrodale, et al. - 2002

Castrodale, et al. created a strut-and-tie model to analyze girders with draped stands and estimate the beam end tension force of a pretensioned girder at release. This model was created to adhere to the requirements of Section 5.10.10.1 in the 1998 edition of AASHTO LRFD. The model presented by Castrodale, et al. ignored the effect of transfer length, applying the prestress force as a concentrated load at the end of the beam. The assumption of 20 ksi working stress in the steel was used in this study.

Findings of this analysis concluded that when the working stress of 20 ksi was used, the area of steel required to resist some larger tension forces would be impossible to implement. The magnitude of the tensile force was higher than the AASHTO LFRD ratio of 4 percent of the prestress force. Castrodale, et al. recognized that this method was conservative and would need further design to create a better model. However, this simple model could be useful to quickly and conservatively evaluate various configurations and reinforcing to control cracking.

2.5.4.3 – Crispino -2007

Crispino (2007) performed research on anchorage zone for prestressed PCBT girders. Crispino performed a parametric study utilizing strut-and-tie modeling to design the end zone reinforcing for various beam sizes and prestressed strand layouts. Through this study, Crispino concluded that for the area between the beam end and $h/4$ had almost identical tension forces as and the area between $h/4$ and $3h/4$. This finding led to the design of a simplified strut-and-tie model with two tension ties that have equal forces. This method was utilized in this thesis, and is shown in detail in Section 6.3.

2.5.5 – Tadros et al. - 2010

Tadros et al. (2010) performed experimental testing for the National Cooperative Highway Researh Program (NCHRP). Testing was performed to investigate if anchorage zone cracking negatively affected the shear and flexural capacities of prestressed girders. Eight 42 ft long full-scale girders were fabricated with different end zone reinforcement details on each end. Each beam end was tested to failure and compared to the predicted failure load.

Tadros et al. concluded that anchorage zone cracking from prestress forces does not cause a negative impact on the structural capacity of the girders. For a few tests, anchorage zone cracks were purposefully created larger than cracks that are commonly observed in industry. Even with these larger cracks, the structural integrity of the girders was higher than the expected capacity. Another finding of this research was the effect of epoxy injection to repair the cracks. It was concluded that the addition of epoxy injection did not significantly increase the capacity of the girders when compared to the girders that did not have epoxy injection repairs on the anchorage zone cracks.

2.6 – Summary

This section has summarized the use of CFRP in beam sections and past research conducted on this subject. There has not been much research on the use of CFRP grids as transverse reinforcement. In order to obtain a cost effective alternative to steel stirrups, the initial cost of CFRP material needs to be reduced. This can be achieved by using it in design alternatives for corrosive environments, which will increase the demand. As demand increases, the availability will increase as well as the cost decreasing. Different methods are available to designers to determine the nominal shear strength of concrete structures. The four methods used in this thesis are AASHTO MCFT, ACI 318, ACI 440.4R, and ACI 440.1R.

Further research is needed with CFRP in anchorage zones and how it can be implemented. VDOT is interested in a steel-less design alternative, and the anchorage zone is a region of increased concerns. The literature review outlines previous methods for designing the anchorage zone region, however, the process has not been done using CFRP grids as the primary reinforcement.

This thesis investigates the use of NEFMAC grid as a viable transverse reinforcement solution as well as implementing Ward's (2016) findings on C-grid. These two materials are used in a preliminary study on anchorage zones and the feasibility of using CFRP grids in this region as reinforcement and to reduce congestion in construction.

3 – Testing Methods

3.1 – NEFMAC Grid Development Tests

3.1.1 – Test Specimens

Previous testing of C-Grid by Ward (2016) was done in the Virginia Polytechnic Institute and State University Structures Lab. Ward's testing was based on testing done on C-Grid by

Ding et. al. (2011). The same set-up was used in this thesis, however, testing was done to determine the development length of NEFMAC grid instead of C-Grid. Testing was done on 4 in., 6 in., and 8 in. development lengths. Two specimens were tested for each development length, for a total of six specimens.

The NEFMAC grid tested was the C6 8 in. x 10 in. spacing, which was the same grid used in the beam tests. The material properties for NEFMAC are provided in Table 1 and the

Table 1: Material Properties for NEFMAC C6

NEFMAC C6	
Tow Area ($in.^2$)	0.027
Tensile Strength (kips)	4.69
Tensile Stress (ksi)	173
Modulus of Elasticity (ksi)	14500

manufacturer provided report of strength is shown in Appendix A. Testing used a minimum of 1.5 in. of clear cover on all sides of the NEFMAC grid to provide a proper cover to reduce the possibility of concrete splitting on the edges. All blocks were 12 in. wide with an 8 in. horizontal spacing between the two longitudinal grids. One transverse tow for each end of grid was present at the same depth into the concrete. The variability in development length was the longitudinal tow lengths of the grid after the transverse tow. Table 2 shows the typical dimensions for the specimens, while Figure 5 shows the typical specimen diagram. Specimen naming convention followed the standard of 4-2, where the 4 represents the inches of embedment of the grid and the 2 indicates the specimen number for that embedment length.

The specimens were placed using wooden formwork. To reduce the possibility of damaging the specimens prior to testing, the base of the formwork was used as the base of the test set-up. The base was split down the middle to ensure friction between the concrete blocks

Table 2: Typical Development Length Specimen Test Matrix

	Dimension (in.)		
Specimen	A	B	C
4-1	1.5	3.5	6
4-2	1.5	3.5	6
6-1	3.5	5.5	8
6-2	3.5	5.5	8
8-1	5.5	7.5	10
8-2	5.5	7.5	10

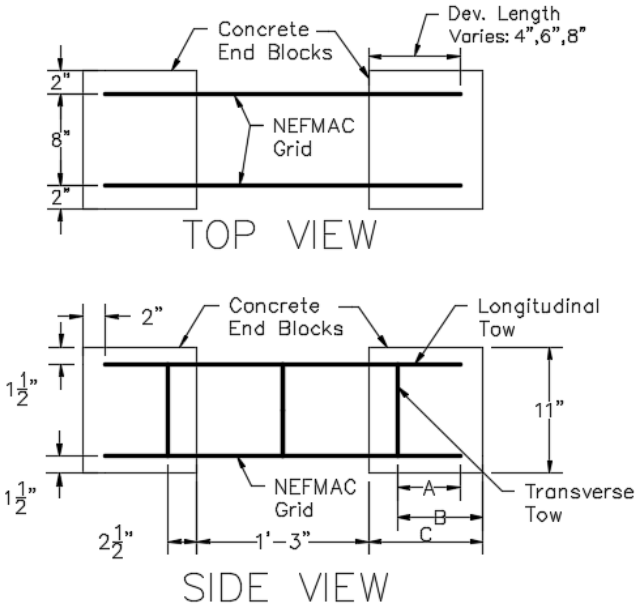

Figure 5: Diagram of Typical Development Length Specimen

and the formwork did not influence the resistance of specimen when the tested on a roller table. The walls of the formwork were designed to be attached at the base as little as possible to ensure removal was easy, reducing the possibility of accidental damage to the exposed grids. Typical formwork for this testing can be seen in Figure 6. The longitudinal walls are the only portion of

the walls that are mechanically attached to the base. The transverse walls were slid between the longitudinal walls and braced in place by the concrete during placement.

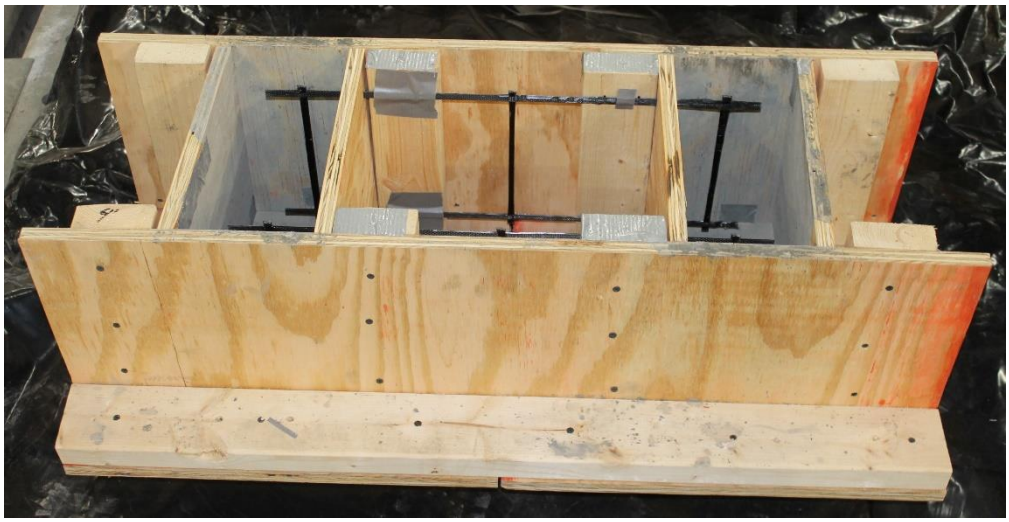

Figure 6: Typical Formwork for Development Length Testing with NEFMAC

3.1.2 – Test Methods

Figure 7 shows the test set-up with instrumentation and collar to catch the specimen upon fracture. Specimen were designed as rectangular prisms of different lengths to allow different embedment lengths. The concrete mix design is provided in Table 3. Concrete used was designed to have a 6-½ in. slump with a 28-day compressive strength of 7000 psi. The concrete was also specified with a maximum aggregate size of ½ in. for easier workability through the NEFMAC material. For less variability in results, concrete for all specimens of the development tests and the beam test were placed from one truck.

Table 3: Concrete Mix Design

Constituent	Amount
#8 Stone	1576 lbs
Natural Sand	1530 lbs
Type I/II Cement	652 lbs
Water	159 lbs
Microsilica	53 lbs
Air Entraining Admixture	1.4 oz
Retarder	24.7 oz
Water Reducing Admixture	28.2 oz
W/C Ratio	0.37

Figure 7: Development Length Set-up

For testing, each specimen was placed on a roller table and then the formwork was removed. As shown in Figure 7, the base was split so that friction of the concrete block against the plywood would have no effect on the test results. Also, difficulty was found in properly aligning the jack in both the vertical and horizontal axes, so that the load was in the middle of the

blocks. A load cell was placed between one block and the jack. Extensometers were attached to each side of the specimen to measure the amount of elongation in the grid. A metal collar was put around the specimen to prevent a dangerous rupture of the NEFMAC grid and test specimen. The tests were conducted by increasing the load until rupture of the grid material between the two concrete blocks or until slippage of the NEFMAC grid through the concrete occurred.

3.1.3 – Instrumentation

Data acquisition was handled by a System 5000 computer system produced by Vishay Instruments. Instrumentation consisted of two Trans-Tek 8 in. barrel LVDTs, and 50 kip load cell. The LVDTs were used to measure elongation of each side of the specimen. To extend the LVDTs across the length of the specimen, PVC pipe extenders were placed across from them. The LVDT data was used to determine if slip in the grid relative to the concrete occurred on either side and also showed the amount of unequal strain in the two sides if loading was not perfectly centered. LVDT brackets and PVC extenders were attached to the blocks with Loctite 410 instant adhesive and Loctite 7452 accelerant. LVDTs were slid through the bracket and then tightened into place via a hose clamp. Figure 8 shows the typical instrumentation used in the test. The load cell is against the left concrete block in the figure.

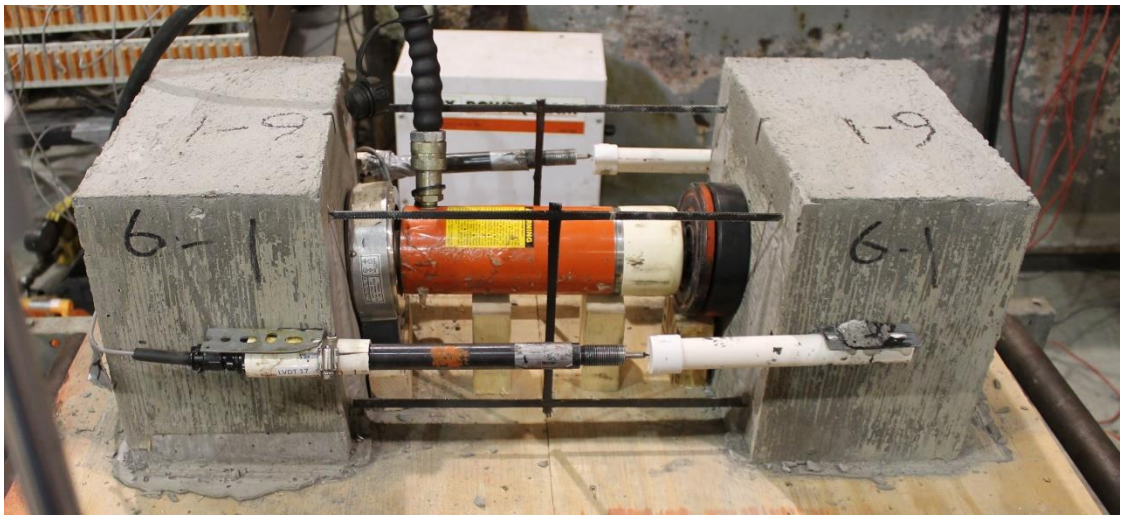

Figure 8: Development Length Instrumentation

3.2 – Beam Test

One beam specimen was created for testing. The beam specimen had a cross-sectional shape based on a typical Bulb-T beam used in highway bridges. The beam was scaled down to 19 in. deep. Two tests were performed on the beam, one on either end.

3.2.1 – Beam Specimen

The beam specimen was a small scale version of Bulb-T beams typically used in highway bridge construction. An Excel spreadsheet was created to calculate the gross section properties and was used to iterate the design to find the final dimensions. Figure 9 shows the cross-section of the beam with major dimensions of the beam.

The beam 18 ft long which allowed for two tests with a span of 12 ft. The beam was a simple span with a roller support at the end and a pin support at the other end. Loading was applied as a single point load 4 ft from the roller support to produce a shear failure and as opposed to flexural failure. The beam was designed so that the end of the beam would represent the

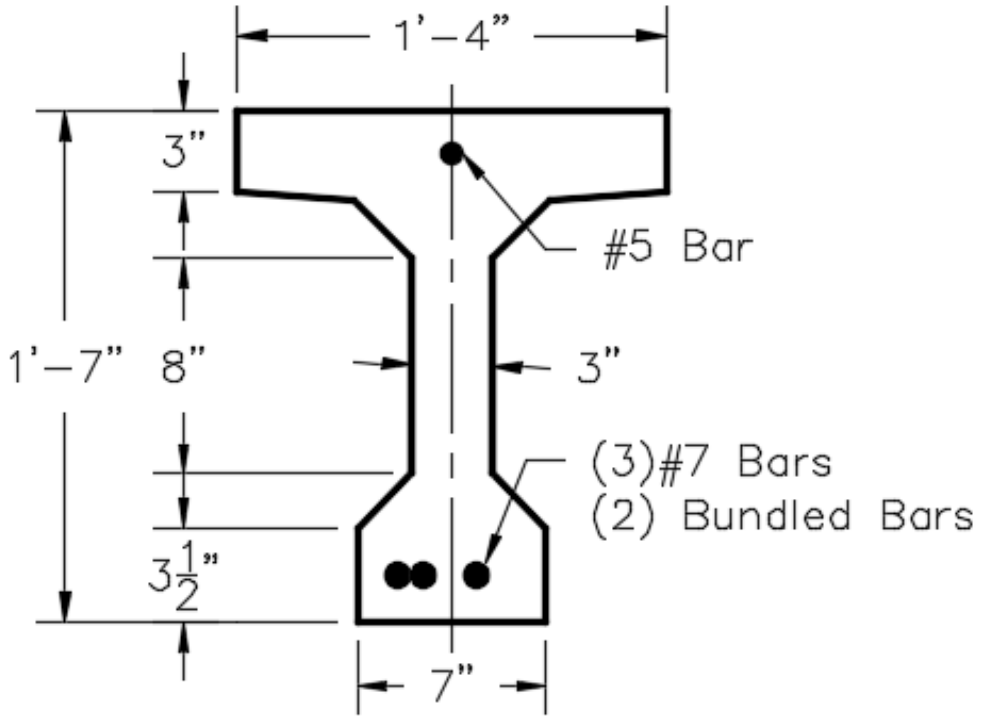

Figure 9: Beam End Elevation

minimum transverse reinforcing ratio used in the section and the other end would represent a typical transverse reinforcement ratio. A spreadsheet that calculated the moment capacity and shear capacity of the beam was created to determine the needed load for shear failure and the amount of longitudinal reinforcing. Additionally, the beam used a top bar in the beam for an anchor point when tying in the transverse reinforcing. Figure 10 shows the test set-up schematic, with the first test on the top and the second test for each beam on the bottom.

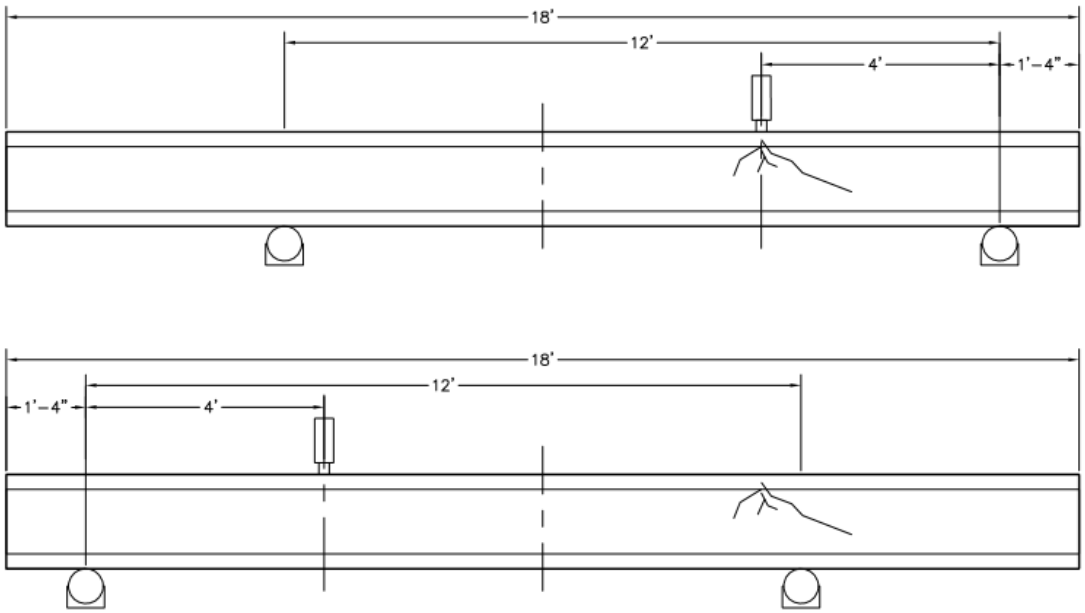

Figure 10: Test Set-up Schematic

Details of the beam specimens are shown in Table 4 along with the anticipated shear strength for each of the transverse reinforcing options in the specimen. These calculations are shown in Appendix B. The minimum specimen was designed following the AASHTO minimum transverse reinforcement provided in Equation 7.

The NEFMAC beam specimen was designed with three No. 7 bars as the bottom tension steel reinforcement to provide a shear failure of the beam prior to flexural failure. A No. 5 bar was used for top compression reinforcement as well as spacing for the two layers of NEFMAC.

Table 4: Beam Specimen Details

Shear Reinforcing	Tow Area (in^2)	Tow Strength (kips)	Spacing (in)	# of Layers	V_n MCFT (kips)	V_n ACI (kips)	Load Point (ft)	Expected Failure Load (kips)
Typ NEFMAC	0.027	4.69	10.0	2	28.5	24.5	4.0	42
Min NEFMAC	0.027	4.69	10.0	1	20.5	16.5	4.0	30

The base of the formwork was assembled first. Then one side of the form was assembled onto the base. Next, 1-¾ in. chairs were placed along the base to provide 2 in. cover for the

longitudinal reinforcing. Next, the No. 7 bars were tied to the chairs. The transverse reinforcing was tied to the bottom longitudinal reinforcing. To ensure adequate transverse reinforcing, splicing of the NEFMAC sheets were used. The splice length was determined by the NEFMAC technical data received with the material (NEFMAC). Figure 11 shows a typical splice length. After the transverse reinforcing was placed, the second side of the formwork was placed. The

Figure 11: Typical Splice Length

transverse reinforcement was tied to the top bar which was held in place by pencil rod anchored through the top of the form. Figure 12 shows completed formwork.

The concrete used was the same mix used by the development length specimens and is described in section 3.1.2. The mix design can be seen in Table 4. The concrete was placed into the form and a pencil vibrator was used to consolidate the concrete. After consolidation, magnesium floats were used to provide a smooth finish to the beam. The concrete was covered with plastic and cured for 7 days. Then, the form was removed to ensure shrinkage of the concrete did not bind the concrete and the form. After form removal the beam was allowed to air cure for additional time until the concrete strength was high enough to test.

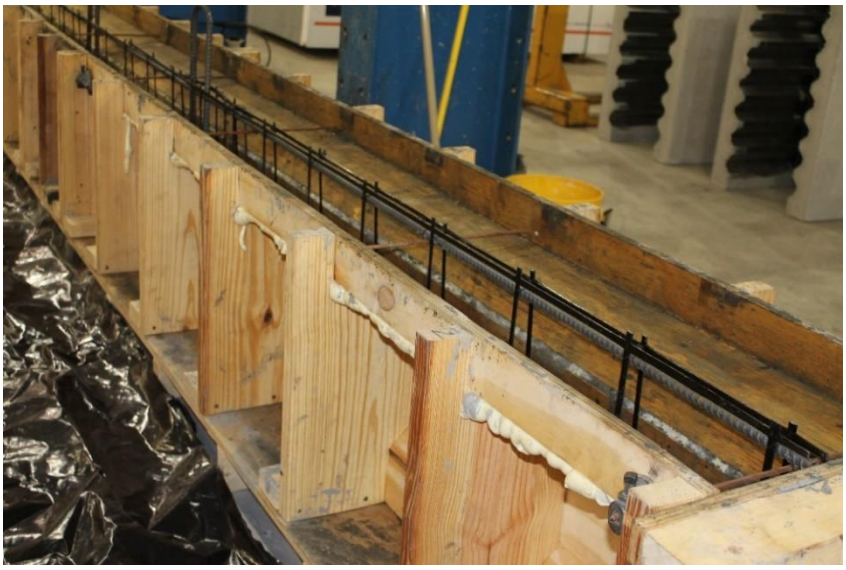

Figure 12: Completed Beam Specimen Formwork

3.2.2 – Test Set-Up

Testing was performed in the VT structures lab on the large beams that act as an additional testing area when the primary strong floor in the lab is busy. Two W 21x73 beams were clamped to the raised beams in the lab 12 ft apart. The frame for load application was placed at 4 ft from the roller support of the beam. The loading apparatus was an Enerpac 150 ton hydraulic ram held in place by columns and channels as shown in the figure. The ram was used with an SPX Power Team hydraulic pump. The complete testing frame set-up is shown in Figure 13.

The beam was simply supported with a roller support and pin support at the ends. The roller and pin were greased prior to testing to reduce friction. Before the beam was set on the rollers a rubber pad was used to help distribute the load along any imperfections in the concrete. Also, the load from the hydraulic ram was transferred to the beam via a set of steel plates with a

Figure 13: Overview of Test Set-up

neoprene bearing pad. This was used to increase the area of applied load on the concrete and to increase the amount of travel the ram could undergo when in contact with the beam. The loading plates and supports used during testing are shown in Figure 14 through Figure 16.

Figure 14: Loading Plates under Hydraulic Ram

Figure 15: Pin Support for Beam End

Figure 16: Roller Support for Beam End

3.2.3 – Instrumentation on Beams

Data from the tests were gathered via a System 5000 computer system made by Vishay Instruments. All instrumentation was calibrated before testing. The load cell was calibrated using the Forney concrete compression testing machine at the structures lab.

The test used three wire potentiometers produced by Measurement Specialties to measure the vertical deflection of the beam. Two were placed near the support at each end of the beam and the third was placed directly under the loading point. This measured true deflection of the concrete beam by accounting for any deflection at the steel support beams. Wire potentiometers were attached to concrete blocks and placed on the floor. The concrete blocks were used to keep the wire potentiometers from moving during testing. Metal shim plates were glued to the beam using Loctite 410 instant adhesive and Loctite 7452 accelerant. Magnetic hooks were then applied to these plates and the string from the wire potentiometer was attached to the hook as shown in Figure 17.

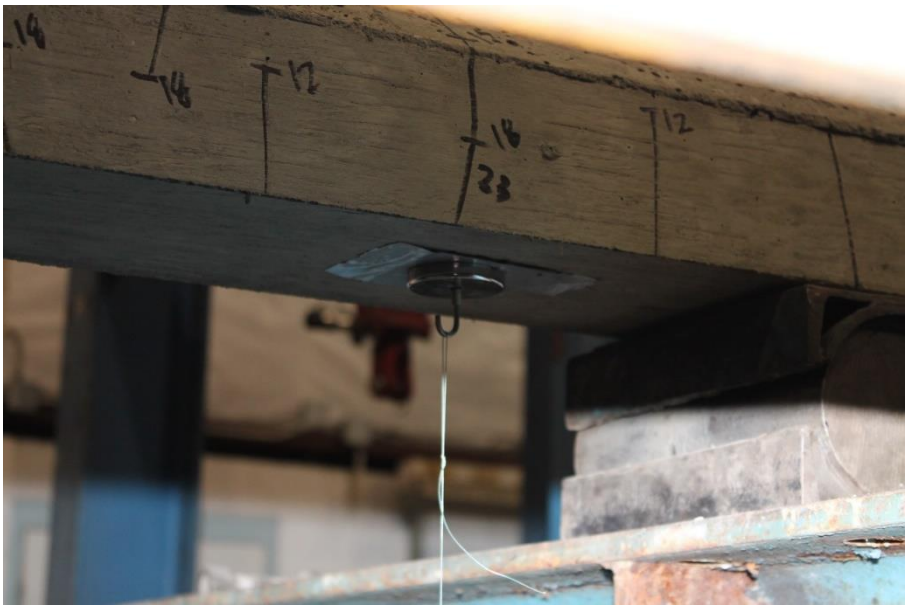

Figure 17: Typical Wire Potentiometer Hook Attachment

On one side, the beam was fitted with four Trans-Tek 0350-0000 LVDTS that measured the web of the beam to capture shear cracking. These four LVDTs were aligned with the vertical tows of the NEFMAC within the shear region. These were attached to the tapered portion of the beam via a wood bracket with metal channel and again used the Loctite adhesive. The typical LVDT crack gage layout for each test is shown in Figure 18.

The other side of the beam used Bridge Diagnostic Inc. strain transducers (BDIs) for crack measurements. The BDIs were arranged along the vertical tows of the NEFMAC similar to the LVDTs. However, the BDIs were staggered vertically to try and capture the shear crack along the entire shear failure. After testing the minimum NEFMAC grid beam, one additional BDI was added for the typical reinforcement test to increase chances of capturing the shear crack. The BDIs attached to the beam via metal feet that are glued to the beam using the same Loctite adhesive. The BDI crack gages for each test are shown in Figure 19 and Figure 20. The full instrumentation plan for the beam is shown in Figure 21.

Figure 18: Typical LVDT Crack Gage Set-up for Testing

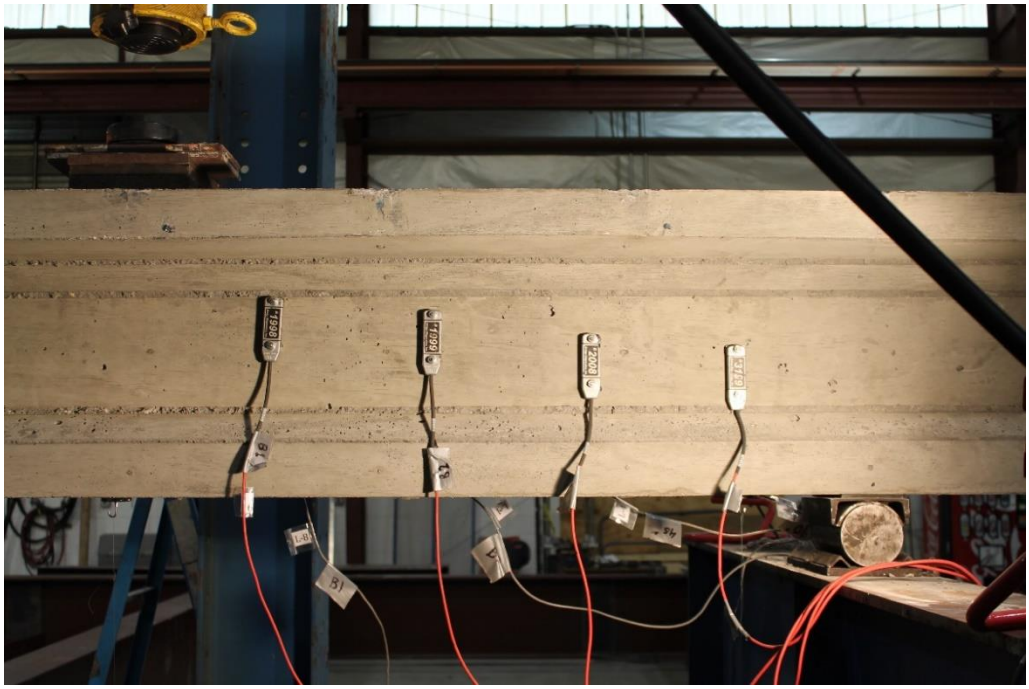

Figure 19: Bar Strain Set-up for Minimum Reinforcement Testing

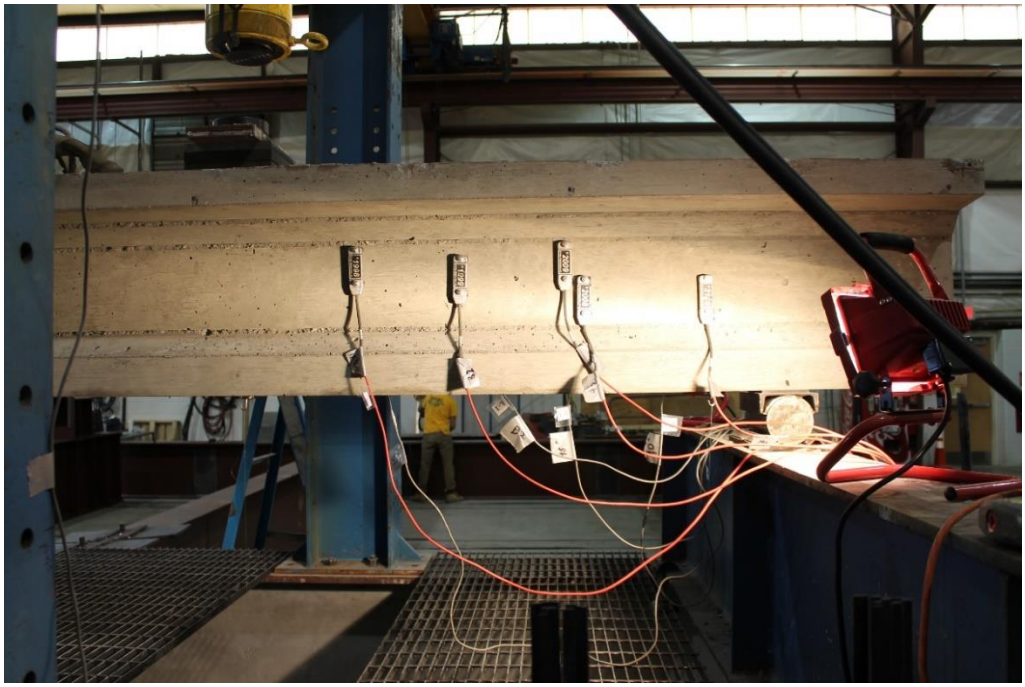

Figure 20: Bar Strain Set-up for Typical NEFMAC Testing

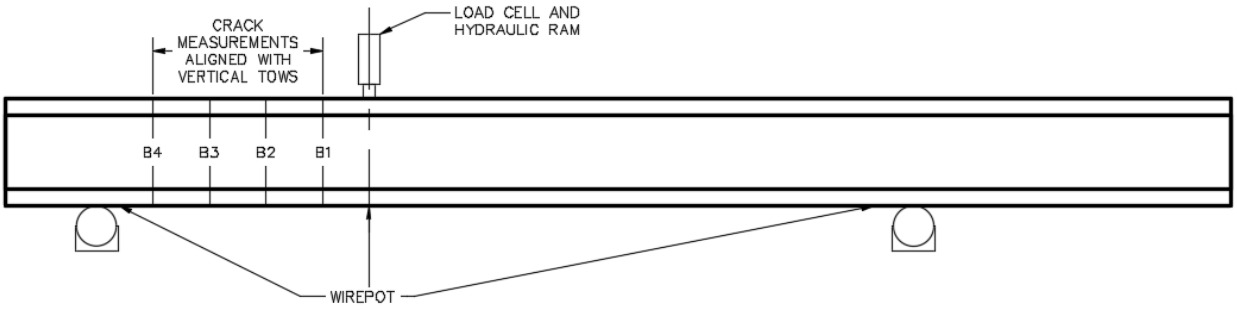

Figure 21: Full Instrumentation for Shear Testing

4 – Test Results

4.1 – Concrete Material Test Results

The concrete used in the beam tests and development tests was specified as a 28 day compressive strength of 7,000 psi concrete. The concrete was required to have a slump of 6 to 8 in. and ½ in. aggregate size to increase the workability. The concrete was purchased from the local ready-mix concrete plant and delivered to the lab. Prior to placement the slump was taken and found to be 6 in. During placement, 4 in. by 8 in. cylinders were cast to be used for concrete material testing. Compressive tests were run following ASTM C39 protocol and splitting tensile followed ASTM

Table 5: Concrete Properties for Tests at Time of Testing

	Compressive Strength f'_c (psi)	Tensile Strength f_t (psi)	Modulus of Elasticity (ksi)
Development Length Test	7490 (3)	565 (3)	4530 (2)
Beam Test	6340 (3)	435 (2)	4900 (2)

C496 protocol in a Forney concrete compression testing machine. The concrete strengths for the development length test and the beam tests are shown in Table 5. A complete report of the concrete data is provided in Appendix C.

4.2 – NEFMAC Grid Development Length Results and Discussion

4.2.1 – NEFMAC Grid Development Length Specimen Results

Six development tests were run with NEFMAC grid. These results are presented in Table 6. The first specimen tested, 4-1, had a slight issue during testing. When the concrete was placed, a portion of the formwork was pushed out of alignment. This misalignment resulted in a bending force in addition to an axial force to be applied to the concrete blocks. This resulted in an applied load slightly smaller than the predicted rupture load of the NEFMAC grid. The failure for specimen 4-1 is shown in Figure 22. The bending of the NEFMAC grid can be seen on the far side of the specimen.

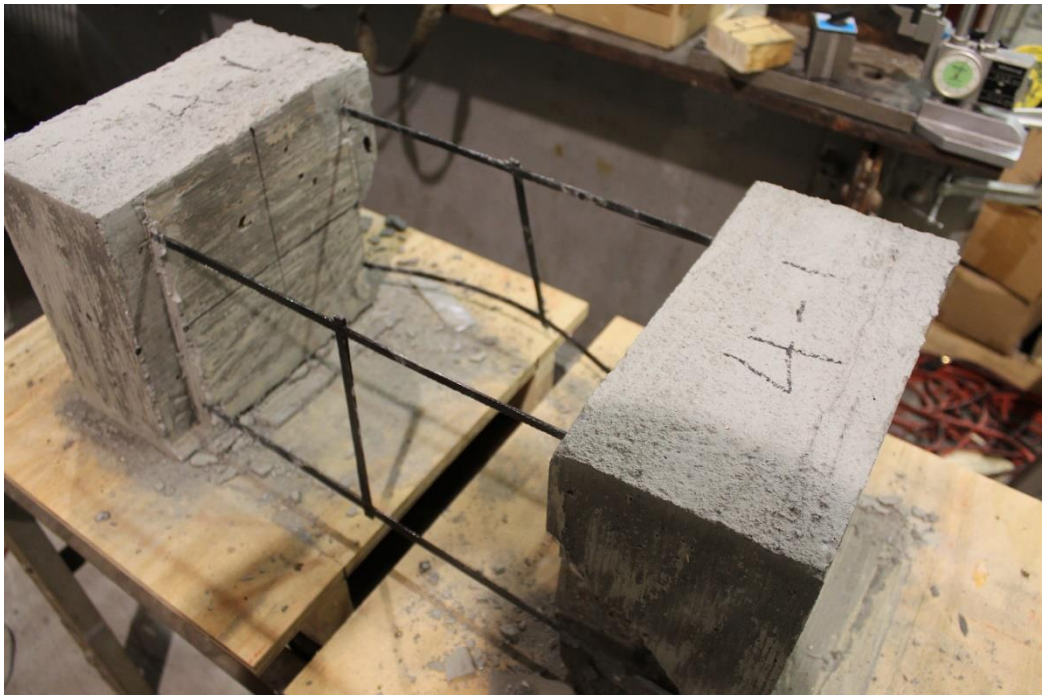

Figure 22: Failure of Specimen 4-1

For the remainder of the specimens, this error was not an issue, since the formwork was not misaligned during the concrete placement. The five remaining development test specimens only had axial forces applied. During the testing of specimens 4-2 and 8-1, the NEFMAC grid only ruptured on one side of the specimen. This was most likely due to the jack not being perfectly centered. Even though only one side ruptured, there was not any apparent slippage of the grid. For specimen 6-2, there was an error with the LVDTs. During the testing, it was noted that the glue holding the LVDTs in place in the metal brackets failed, showing a larger displacement in the graph than what actually occurred. The LVDT data for this test was unusable, however, it is apparent that this test reached full development in the grid due to the failure load matching closely to the predicted failing load.

To analyze the data, the load and two displacements obtained by the testing equipment were put into a spreadsheet on Excel. For each specimen, graphs were produced to show the load versus displacement for both sides of each specimen. If slipping occurred in the specimen, the graphs would have a sudden change in the positive slope. However, none of the specimens had slippage, so this was not seen. A typical plot from this testing is shown in Figure 23, and the remaining plots are shown in Appendix D.

As shown in Table 6, the average failure load of the grid was 17.4 kips. NEFMAC manufacturers reported each tow in the grid has a tensile strength of 4.69 kips. There are two tows of the grid present on each side of the specimen in the development testing set-up, creating a failure load of 9.38 kips per side, or 18.8 kips total.

Even though the 18.8 kips expected failure was greater than the average failure of 17.4

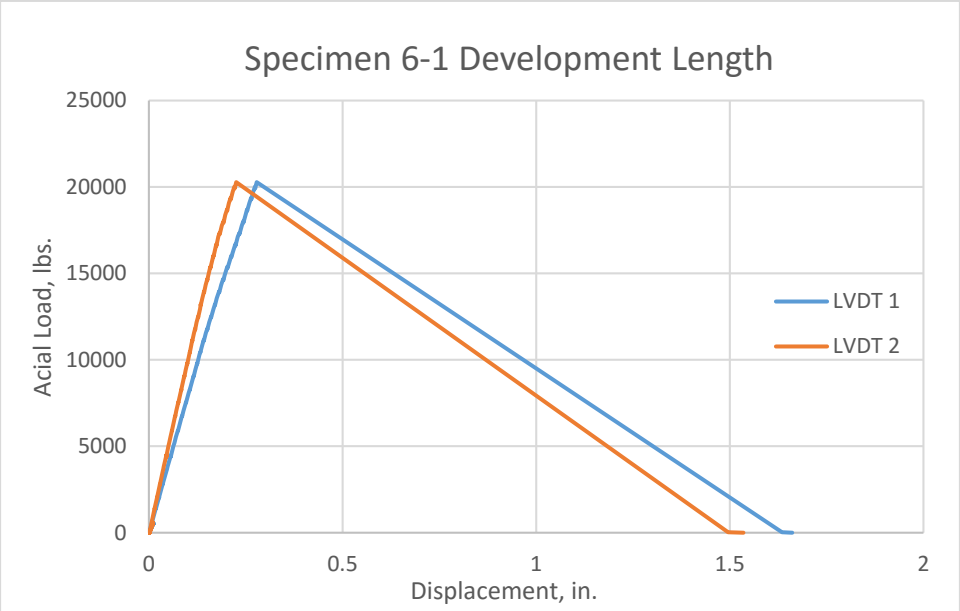

Figure 23: Typical Development Length Plot

kips, there was no measured slipping in the testing. This difference in strength at failure is a result of the testing set-up. For the testing, the loading was not applied directly in the center of the specimens, so there was an unequal force applied to each grid. As shown in Table 6, there is a difference in the 'Load per Side' for each specimen. This column tabulates the estimated load on each side the of the specimen—or the load per two tows of NEFMAC grid. The estimated load on each side was determined from the percent difference in LVDT displacement on each side. When one side of the specimen elongated more, then the estimated load for that side was increased. Based on manufacturer's reported data, two tows of grid should fail at 9.38 kip of loading. The last column of Table 6, '% from Failure', takes the larger value from the 'Load per Side' portion, and outputs the difference between the reported failure load of 9.38 kips and the tested failure load. This was done to provide results on how closely one grid in the specimen was to the predicted failure load when it failed. A positive value in this column represents a tested failure strength that was greater than the 9.38 kips provided failure load. Throughout the

tests, the average failure was 7.65% larger than manufacturer's reported failure load. For the two specimens that failed prior to reaching the predicted failure load, 4-1 and 8-1, other factors could have caused the premature failure. As discussed above in this section, specimen 4-1 had error due to the formwork. This error created a large unequal loading in the grid that caused the

Table 6: Development Testing Results

			LVDT 1		LVDT 2		% Difference		Load per Side (lbs)		% from Failure
Test	Max Load (lbs)	Slip	1000 lbs	15000 lbs	1000 lbs	15000 lbs	1000 lbs	15000 lbs	Left	Right	
4-1	15081	No	0.0122	0.165	0.0154	0.189	20.6	12.5	8480	6600	-9.59
4-2	17875	No	0.00661	0.163	0.0136	0.209	51.5	21.9	6980	10900	16.20
6-1	20279	No	0.0170	0.195	0.0140	0.153	21.1	27.5	12900	7350	37.53
6-2*	18098	No	-	-	-	-	-	-	-	-	-
8-1	16073	No	0.0114	0.167	0.0101	0.161	12.8	3.5	8320	7760	-11.30
8-2	17651	No	0.0143	0.176	0.0140	0.157	2.2	12.0	9890	7760	5.44
Average	17392		0.0123	0.173	0.0134	0.174	21.7	15.5			7.65

*** indicates specimen was not included in average**

failure prematurely. For specimen 8-1, the loading was most likely off center, providing a load that was not purely axial loading. Figure 24 plots the development length versus the failure load for each test. Since the trendline is almost horizontal, there was no change in failure loads between the different development lengths. Based on the results presented in Table 6 and Figure 24, NEFMAC grid was fully developed at a 4 in. development length.

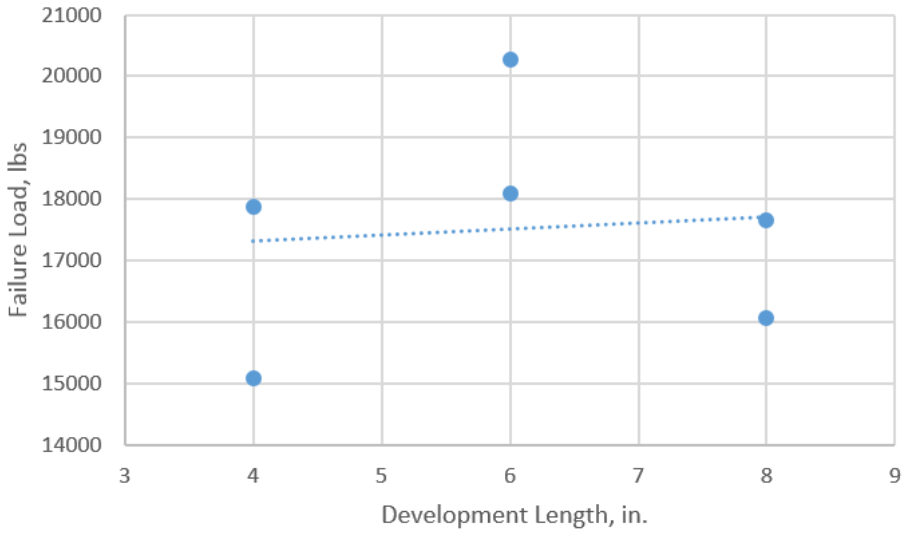

Figure 24: Development Length vs. Failure Load

4.3 – NEFMAC Grid Beam Tests and Discussions

4.3.1 – Discussion on BDI Data

The BDI data obtained during testing of the beam specimens was not used in these results. The data obtained through these instruments was inconsistent. BDI gages have a maximum displacement of 0.008 in., therefore, after cracks formed larger than this the data obtained was inaccurate and noisy. Prior to shear cracking, the information obtained from the BDIs were valid, however, the cracking occurred early in each test. In addition, when the shear cracks were large enough some of the BDIs would partially detach from the beam, causing more inaccurate readings.

4.3.2 –Minimum NEFMAC Reinforcement

The minimum NEFMAC grid reinforcement was composed of one layer of C6 10x8 grid that was placed the entire length of the beam section. The 10 in. spacing was the spacing of the vertical legs of the grid that acted as stirrups. The cross-section of the specimen is shown in Figure 25. The load was applied at 4 ft from the support on a 12 ft span. Using the AASHTO MCFT method, the predicted loading for shear failure for this test was 30 kips.

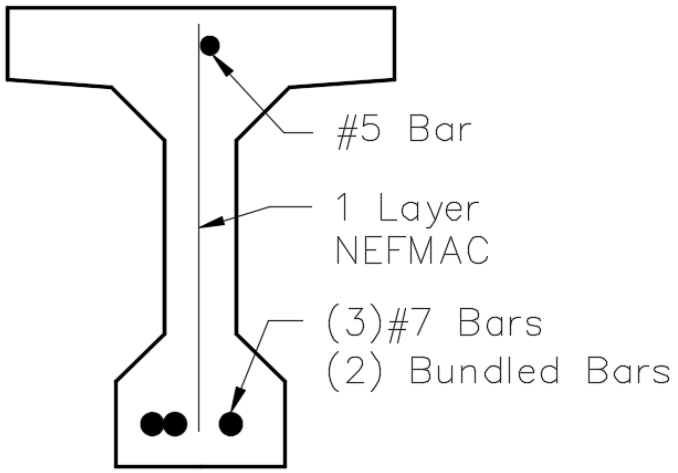

Figure 25: NEFMAC Grid Minimum Reinforcement Cross-Section

Load was applied to the beam until it reached its predicted failure load in 3 kip increments. The vertical deflection of the beam at the load point can be seen in Figure 26. At the predicted failure load, testing was stopped to ensure that damage to the typical reinforcement side of beam was minimal.

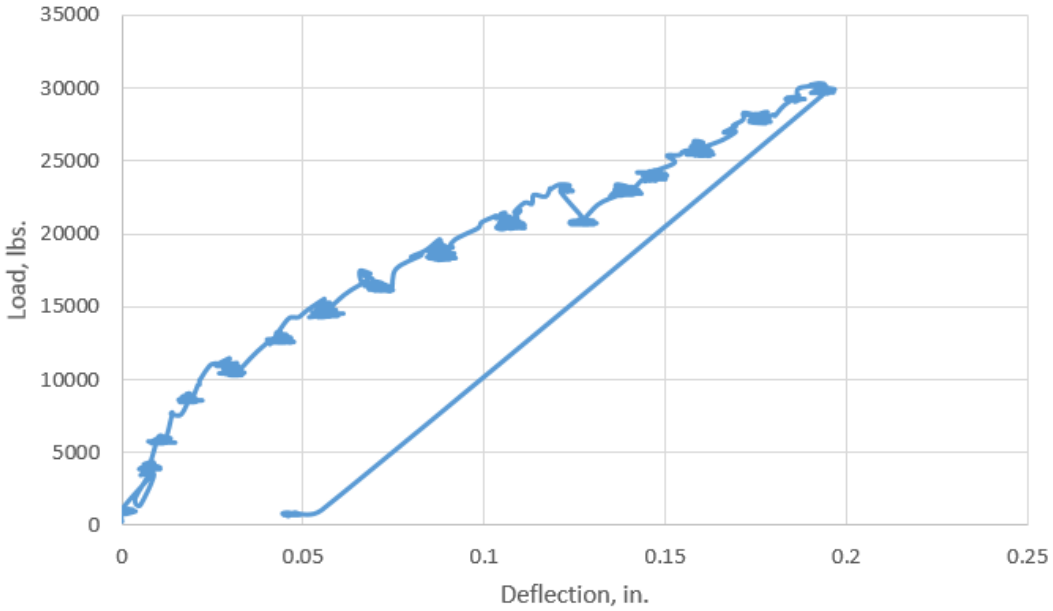

Figure 26: Load versus Deflection at Load-Point for Minimum NEFMAC

After testing of the typical reinforcement side, the minimum reinforcement side was re-loaded and tested to failure (the beam no longer has any load carrying capacity). Load was increased up to 5 kips initially, and then increased by 2-kip increments. Shear failure of the beam occurred at 50 kips, approximately 67% more load than predicted. The beam was then unloaded and the failure crack is shown in Figure 27. Upon closer inspection of the shear crack, visible rupture of the vertical tows could not be seen. However, there was fraying of the vertical tows which may have weakened the grid, as seen in Figure 28.

Figure 27: Unloaded Shear Failure of Minimum NEFMAC-grid Reinforcement

Since the minimum end was tested to failure after the typical end, there was un-seeable damage to the minimum side that could have caused a shear failure without rupture in the vertical tows.

Crack widths were measured for the first two shear cracks to open on this beam. The first crack appeared at a shear loading of about 11 kips, and the second crack appeared at 16 kips. It can be seen in Figure 29 that once the second crack opens, the first crack got smaller. This was because the second crack was the point of shear failure, and resulted in a larger crack opening that forced the first crack to close. Cracks were only measured up until a shear load of 17.5 kips due to 20 kips being the expected shear failure load of for test, and the increase in danger of getting close to measure. The crack propagation along with best fit lines are show in Figure 29.

Figure 28: Fraying of NEFMAC Vertical Tow

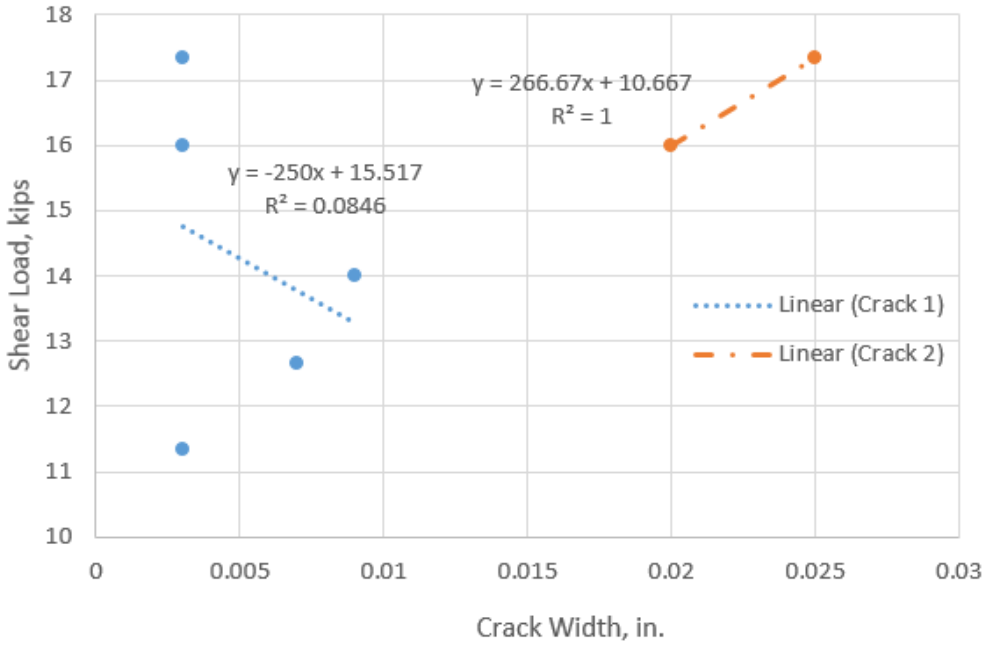

Figure 29: Crack Propagation on Minimum NEFMAC Test

Vertical LVDTs were placed along the vertical tows within the shear failure region. Figure 30 shows the crack propagation relative to the LVDTs. Their displacements are provided in Figure 31. Initial cracking occurred around a shear load of 11 kips based on the LVDT data. However, the larger cracking occurs around 16 kips, which corresponds to the second shear cracking opening. The LVDT readings are indicating larger crack openings than the visual readings. This is due to the LVDT taking into account all of the cracking within the web depth, while the visual reading is of two specific cracks.

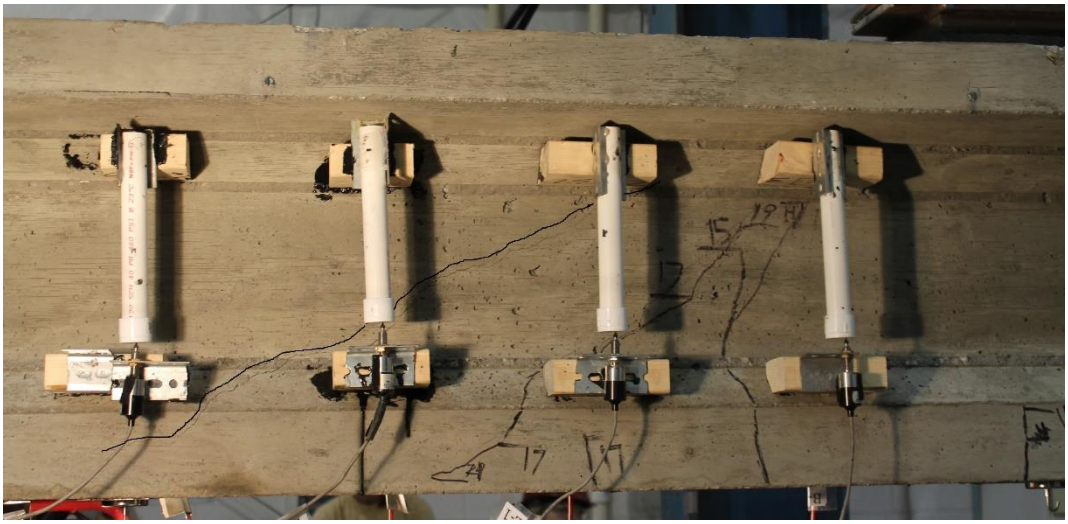

Figure 30: Crack Propagation through LVDTs for Minimum NEFMAC Test

4.3.3 –Typical NEFMAC Reinforcement

The minimum NEFMAC grid reinforcement was composed of two layers of C6 10x8 grid that were placed the entire length of the beam section. The 10 in. spacing was the spacing of the vertical legs of the grid that acted as stirrups. The cross-section of the specimen is shown in Figure 32. The load was applied at 4 ft from the support on a 12 ft span. Base on the AASHTO MCFT method, the predicted loading for shear failure for this test was 42 kips.

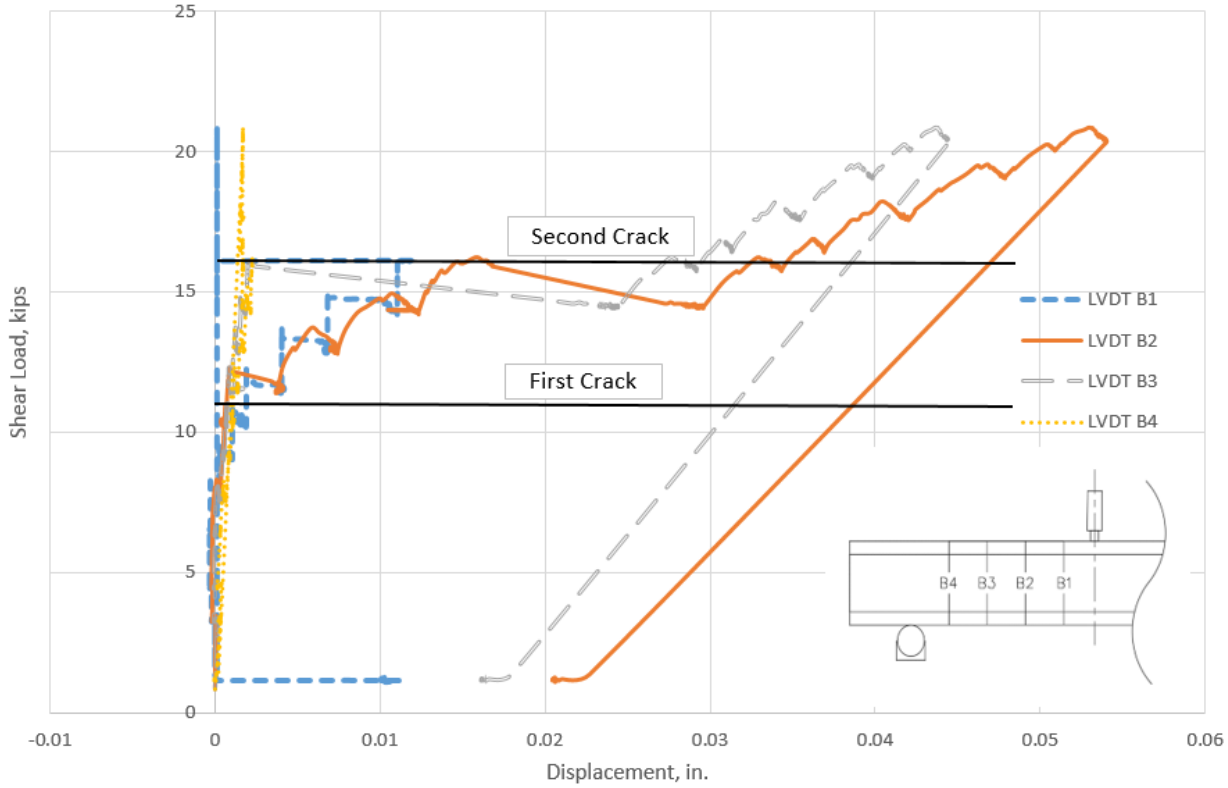

Figure 31: LVDT Displacement of Minimum NEFMAC Test

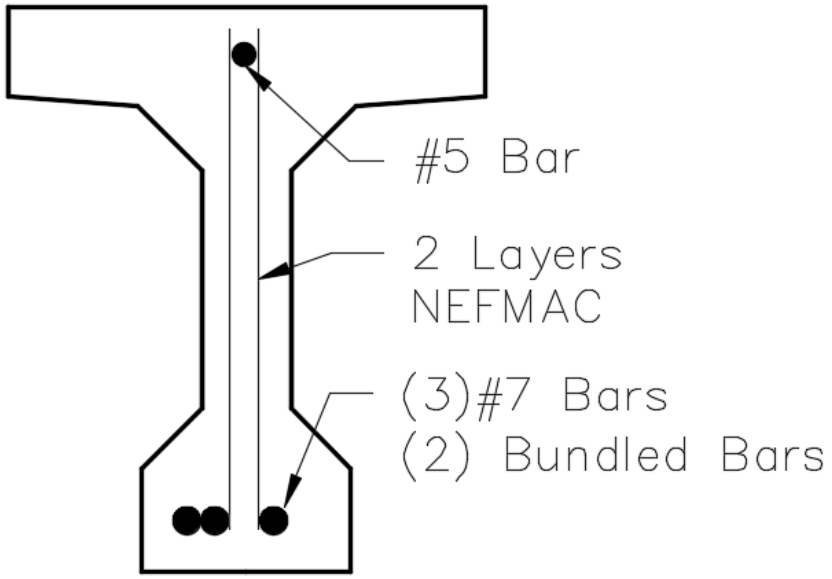

Figure 32: NEFMAC Grid Typical Reinforcement Cross-Section

Loading was applied in 2 to 3 kip increments. Load was applied to the beam until it reached its ultimate failure load. The deflection of the beam at the load point can be seen in Figure 33. Shear failure of the beam occurred at 54 kips, approximately 29% more load than predicted. The beam was then unloaded and the failure crack is shown in Figure 34. Upon closer inspection of the shear crack, visible rupture of the vertical and horizontal tows could be

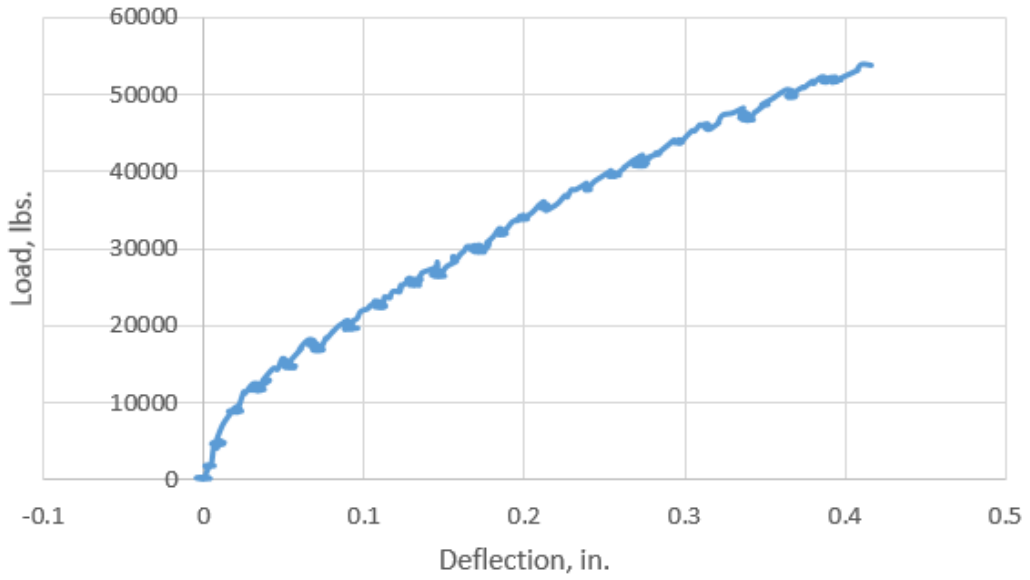

Figure 33: Load Versus Deflection at Load Point for Typical NEFMAC

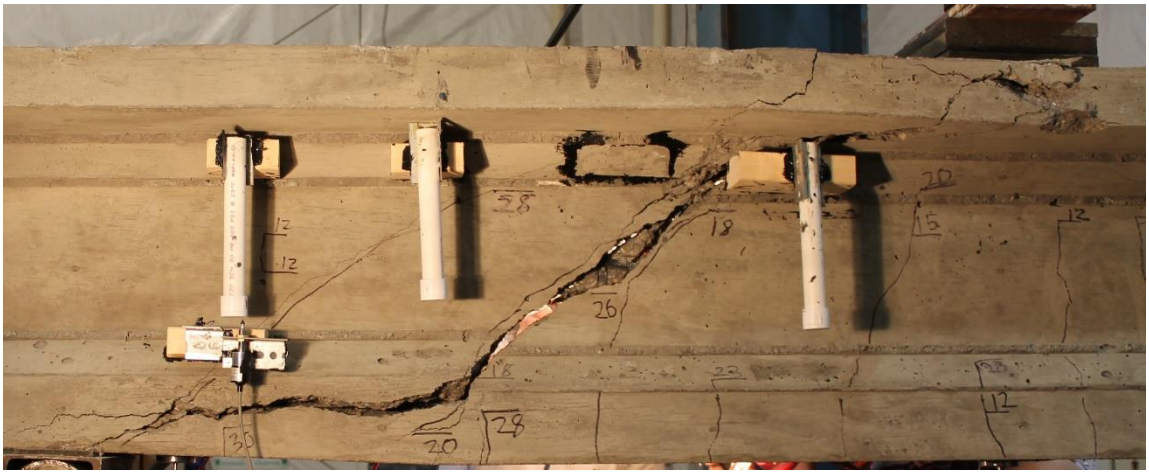

Figure 34: Shear Failure of Typical NEFMAC Reinforcement

seen. Since the vertical tows ruptured completely, the beam specimen failed in shear. This failure of the tows can is shown in Figure 35.

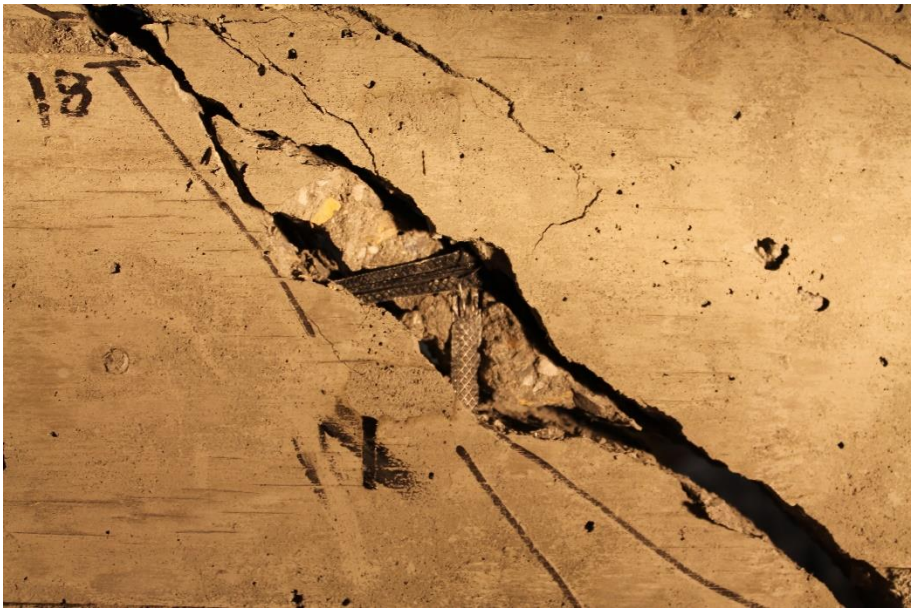

Figure 35: Rupture of Vertical and Horizontal NEFMAC Tows

Crack widths were measured for the first two shear cracks to open on this beam. The first crack appeared a shear loading of 11 kips, and the second crack appeared at 19 kips. Cracks were only measured by hand up until a shear load of 20 kips. The crack propagation along with best fit lines are show in Figure 36.

Vertical LVDTs were placed along the vertical tows within the shear failure region. Figure 37 shows the crack propagation relative to the LVDTs. Their displacements are provided in Figure 38. Initial cracking occurred around a shear load of 12 kips based on the LVDT data, which corresponds to the first visual shear crack opening in Figure 36. Similar to the minimum NEFMAC beam testing, The LVDT readings for the typical NEFMAC beam testing are indicating larger crack openings than the visual readings. This is due to the LVDT taking into

account all of the cracking within the web depth, while the visual reading is of two specific cracks.

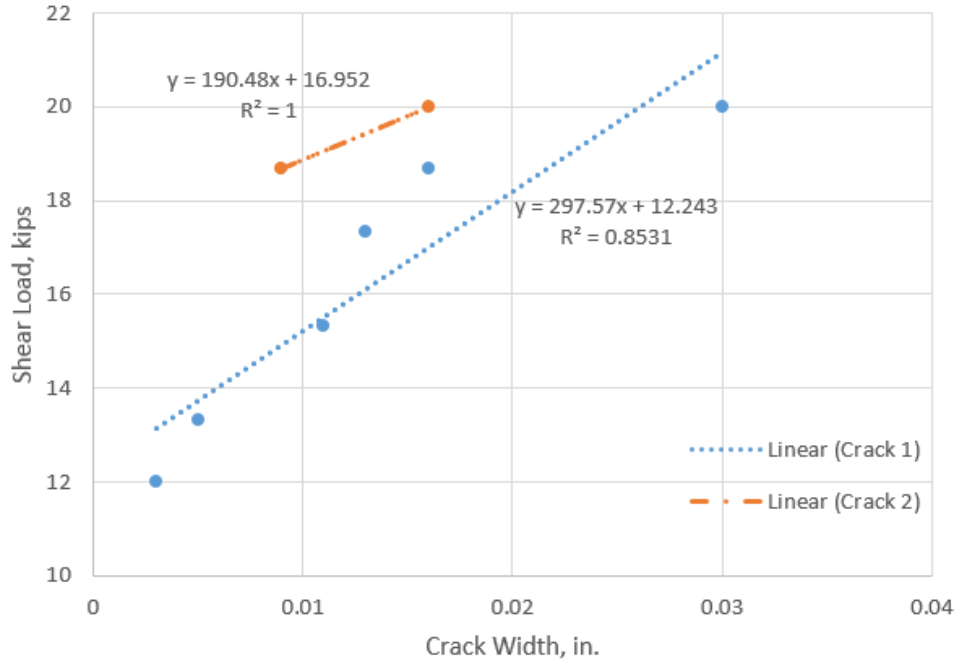

Figure 36: Crack Propagation of Typical NEFMAC Test

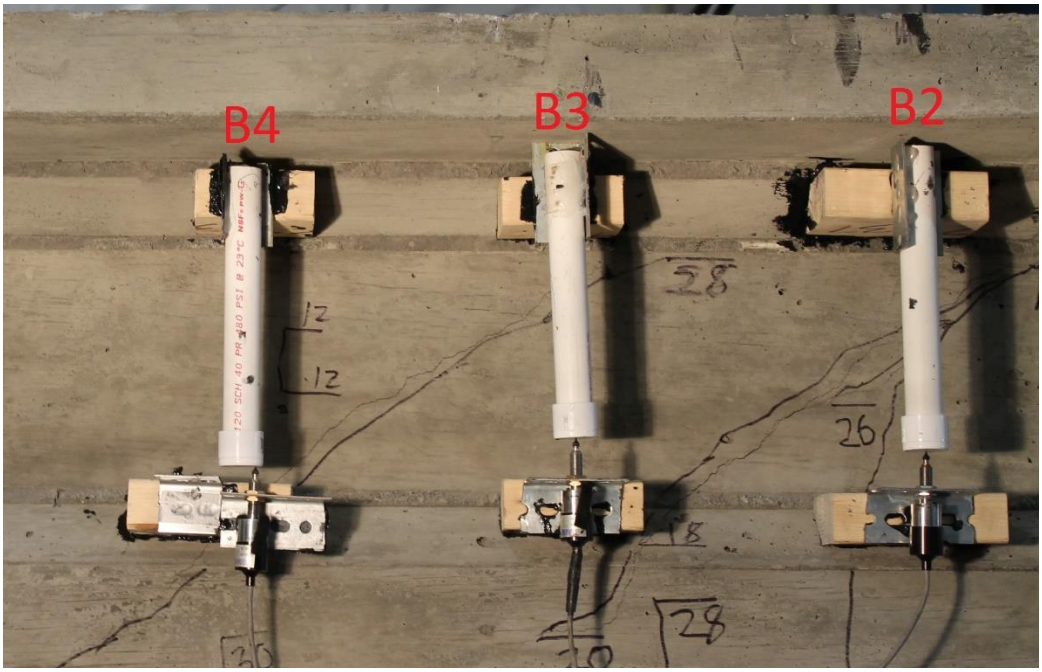

Figure 37: Crack Propagation through LVDTs for Typical NEFMAC Test

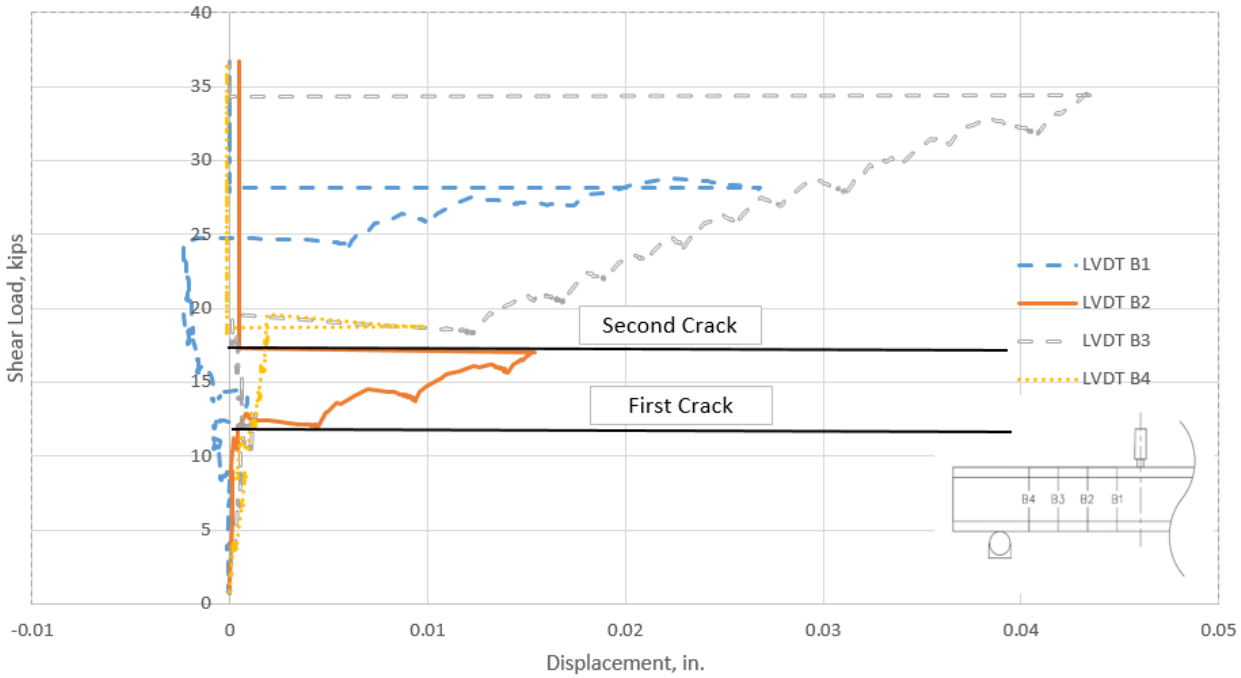

Figure 38: LVDT Displacement of Typical NEFMAC Test

5 – Discussion of Beam Tests

5.1 – Shear Design Methods and Discussion

As discussed in the literature review section of this thesis, four different shear design methods were compared to test results in this thesis. This section discusses the calculated strengths with these methods compared to the actual tested values during the beam tests and evaluates which method provides better prediction of strength for the two beam sections.

The design material values and the actual measured material properties are used for each shear design method. Unless reductions were required by code, NEFMAC grid design material values are taken from the provided specifications that came with the shipment (NEFMAC). The actual properties for the NEFMAC grid were not tested for this thesis, so the manufacturer provided values were taken as the actual values. The NEFMAC values were all the average minus three standard deviations for each property. The actual concrete strength was the

compressive strength of the concrete during testing. The actual steel properties were obtained from Ward (2016) since the same materials were used in this testing. These material properties are summarized below in Table 7.

Table 7: Design and Actual Material Properties

Material and Property	Design	Actual
Concrete f'c	7.0 ksi	6.34 ksi
Steel Yield Stress	60 ksi	59 ksi
Steel Modulus of Elasticty	29000 ksi	29900 ksi
NEFMAC Tow Breaking Stress	173 ksi	173 ksi
NEFMAC Modulus of Elasticity	14500 ksi	14500 ksi

5.1.1 – AASHTO Modified Compression Theory

The AASHTO calculations are discussed in detail in section 2.3.1 of this thesis. Based on section 5.8.2.8 in AASHTO, for design strength, a stress in the shear reinforcement is limited to the minimum of 0.0035 times the modulus of elasticity of the material with a maximum of 75 ksi and the yield/breaking stress of the material. The NEFMAC grid maximum strength is limited by modulus of elasticity times 0.0035. The values for maximum allowable stress for NEFMAC and steel are presented below in Table 8.

Table 8: AASHTO Maximum Reinforcement Stresses

Design Values (ksi)			
Material	f_y or f_u	0.0035E	f_{max}
Steel	60	102	60
NEFMAC	173	50.8	50.8
Actual Values (ksi)			
Material	f_y or f_u	0.0035E	f_{max}
Steel	59	105	59
NEFMAC	173	50.8	50.8

A summary of the AASHTO design calculations are provided in Table 9. A ratio of V_{test}/V_u equal to 1 indicates a design shear load at failure identical to the tested shear load at failure. For both tests, the AASHTO design method is very conservative as seen by the ratios for tested shear load failure to the design shear load failures. Since the ratios are all much greater than 2, it would be safe but uneconomical to use this method.

Table 9: AASHTO MCFT Design Strength Results

Shear Reinforcing	V_n-Design (kips)	V_n-Actual (kips)	Max Shear Load (kips)	Failure	Ratio V_{test}/V_n-Design	Ratio V_{test}/V_n-Actual
Min NEFMAC	12.3	13.9	34.2	Yes, Shear	2.77	2.45
Typ NEFMAC	13.5	16.5	36.7	Yes, Shear	2.71	2.23

5.1.2 – AASHTO Modified Compression Theory Using Full Strength

The AASHTO method limits the maximum stress in the reinforcing which provided overly conservative nominal shear calculations. The calculations were duplicated without taking the limits of maximum stress in consideration. This provided a way to see how the full strength (strength of the NEFMAC grid without any code limitations on stress) of the NEFMAC grid, as reported by the manufacturers, can be utilized in the AASHTO method. The full strength is the tow breaking stress presented in Table 7. As reported by the manufacturer, this strength is the average tensile strength minus three standard deviations. A summary of the full strength AASHTO method calculations are provided in Table 10.

Table 10: AASHTO MCFT Full Strength Results

Shear Reinforcing	V_n-Design (kips)	V_n-Actual (kips)	Max Shear Load (kips)	Failure	Ratio V_{test}/V_n-Design	Ratio V_{test}/V_n-Actual
Min NEFMAC	20.2	19.8	34.2	Yes, Shear	1.69	1.72
Typ NEFMAC	28.1	27.8	36.7	Yes, Shear	1.31	1.32

From Table 10, it is apparent that the calculations provide a good fit, especially for the typical NEFMAC test. This method is still conservative, but not as much as the AASHTO method with the stress limitations. The typical NEFMAC's design using full strength of the grid is a good fit and would lead to a more economical but still safe design.

5.1.3 – ACI 318 Shear Theory

The ACI 318 design process is outlined in detail in section 2.3.2 of this thesis. A limit is set for maximum stress in the grid of 80 ksi, which is the maximum stress for welded wire mesh. The steel longitudinal reinforcement has a maximum stress of 60 ksi. Maximum stresses for the shear design are presented in Table 11.

Table 11: ACI 318 Maximum Reinforcement Stresses

Design Values (ksi)		
Material	f_y or f_u	f_{max}
Steel	60	60
NEFMAC	173	80
Actual Values (ksi)		
Material	f_y or f_u	f_{max}
Steel	59	59
NEFMAC	173	80

The results of Table 12 show that this method does not provide a good estimate for the actual shear strength of the beams. Ratios of greater than 2 for all cases indicate the method is overly conservative in calculating the capacity of sections with NEFMAC grid shear reinforcement.

Table 12: ACI 318 Design Strength Results

Shear Reinforcing	V_n-Design (kips)	V_n-Actual (kips)	Max Shear Load (kips)	Failure	Ratio V_{test}/V_n-Design	Ratio V_{test}/V_n-Actual
Min NEFMAC	12.1	11.8	34.2	Yes, Shear	2.83	2.90
Typ NEFMAC	15.7	15.5	36.7	Yes, Shear	2.34	2.37

5.1.4 – ACI 318 Shear Theory Using Full Strength

The ACI 318 method limits the maximum stress in the NEFMAC reinforcing to 80 ksi which provided overly conservative nominal shear calculations. Therefore, this section compares tests to the ACI 318 method of shear design using the full manufacturer's reported strength of the NEFMAC grid. As reported by the manufacturer, this strength is the average tensile strength minus three standard deviations.

Table 13: ACI 318 Full Strength Design

Shear Reinforcing	V_n-Design (kips)	V_n-Actual (kips)	Max Shear Load (kips)	Failure	Ratio V_{test}/V_n-Design	Ratio V_{test}/V_n-Actual
Min NEFMAC	16.3	15.9	34.2	Yes, Shear	2.09	2.15
Typ NEFMAC	24.2	23.8	36.7	Yes, Shear	1.51	1.54

NEFMAC grid. The table shows that this method is overly conservative, but not as much as using the limitations of stress. For the typical NEFMAC reinforcement, since the ratio for tested failure load to nominal failure load is around 1.5, this method yields a design about 50% over reinforced. This allows for a safe design, but somewhat uneconomical design.

5.1.5 – ACI 440.4R Shear Theory

The ACI 440.4R method is used in the design of prestressed FRP members. Testing in this thesis did not involve prestressed members, however, understanding this method with the use of FRP shear reinforcement is important for future design.

The ACI 440.4R method is outlined in section 2.3.3 of this thesis. The method limits the maximum stress of the material to 0.002 times the elastic modulus, the guaranteed tensile

strength, or the bend radius reduction strength. The maximum reinforcment stresses are shown in Table 14.

Table 14: ACI 440.4R Maximum Reinforcement Stresses

Design Values (ksi)				
Material	f_{fu}	f_{fb}	0.002E	f_{max}
Steel	60	-	58	58
NEFMAC	173	-	29	29
Actual Values (ksi)				
Material	f_{fu}	f_{fb}	0.002E	f_{max}
Steel	59	-	60	59
NEFMAC	173	-	29	29

The results of the shear capacity calculations are presented in Table 15. The ACI 440.4 method is extremely conservative, yielding design strengths that are greater than three times the tested strength. This shows that the ACI 440.4 method is a very safe but very uneconomical design when prestressing is not used.

Table 15: ACI 440-4R Design Strength Results

Shear Reinforcing	V_n-Design (kips)	V_n-Actual (kips)	Max Shear Load (kips)	Failure	Ratio V_{test}/V_n-Design	Ratio V_{test}/V_n-Actual
Min NEFMAC	9.75	9.45	34.17	Yes, Shear	3.50	3.62
Typ NEFMAC	11.07	10.78	36.67	Yes, Shear	3.31	3.40

5.1.6 – ACI 440.4R Shear Theory Using Full Strength

The ACI 440.4R method limits the maximum stress in the NEFMAC reinforcing to 29 ksi which provided overly conservative nominal shear calculations. Therefore, this section compares tests to the ACI 440.4R method of shear design using the full strength reported by the manufacturer. Again, this strength is the average tensile strength minus three standard deviations.

Table 16: ACI 440.4R Full Strength Design

Shear Reinforcing	V_n-Design (kips)	V_n-Actual (kips)	Max Shear Load (kips)	Failure	Ratio V_{test}/V_n-Design	Ratio V_{test}/V_n-Actual
Min NEFMAC	16.3	15.9	34.2	Yes, Shear	2.09	2.15
Typ NEFMAC	24.2	23.8	36.7	Yes, Shear	1.51	1.54

Table 16 presents the calculations using the full strength and the ACI 440.4 method. This method obtained the same results as ACI 318 full strength calculations above because there is no prestressing present in the design. Since the values obtained with the design strength are overly conservative compared to ACI 318, this not recommended for design.

5.1.7 – ACI 440.1R Shear Theory

The ACI 440.1 method is described in section 2.3.3 of this thesis. The method limits the maximum stress of the material to 0.004 times the elastic modulus, the guaranteed tensile strength, or the bend radius reduction strength. The maximum reinforcement stresses are shown in Table 17.

Table 17: ACI 440.1R Maximum Reinforcement Stresses

Design Values (ksi)				
Material	f_{fu}	f_{fb}	0.004E	f_{fv}
Steel	60	-	116	60
NEFMAC	173	-	58	58
Actual Values (ksi)				
Material	f_{fu}	f_{fb}	0.004E	f_{fv}
Steel	59	-	120	59
C-Grid	173	-	58	58

Table 18 below presents the ACI 440.1 design strength calculations and results. Since the ratios are all far greater than 1, this method is conservative. The method will lead to a safe but somewhat uneconomical design.

Table 18: ACI 440.1R Design Strength Results

Shear Reinforcing	V_n-Design (kips)	V_n-Actual (kips)	Max Shear Load (kips)	Failure	Ratio V_{test}/V_n-Design	Ratio V_{test}/V_n-Actual
Min NEFMAC	18.5	17.8	34.2	Yes, Shear	1.85	1.92
Typ NEFMAC	21.2	20.5	36.7	Yes, Shear	1.73	1.79

5.1.8 – ACI 440.1R Shear Theory Using Full Strength

The ACI 440.1R method's limitations to stress provide designs that have about 75-90% more shear capacity than calculated. To obtain a less conservative design, the ACI 440.1 method is used with the full strength of the tows. Again, the NEFMAC full strength is the average reduced by three standard deviations to ensure a safe design. The steel longitudinal reinforcement strength was not originally affected by the stress limitations, so it does not change for the full strength calculations.

Table 19: ACI 440.1R Full Strength Results

Shear Reinforcing	V_n-Design (kips)	V_n-Actual (kips)	Max Shear Load (kips)	Failure	Ratio V_{test}/V_n-Design	Ratio V_{test}/V_n-Actual
Min NEFMAC	23.8	23.0	34.2	Yes, Shear	1.44	1.49
Typ NEFMAC	31.7	30.9	36.7	Yes, Shear	1.16	1.19

From the calculations presented in Table 19, there is good correlation between full strength design and tested failure load since the ratios are close to 1. This method provides a safe and economical design for these tests.

5.1.9 – Summary of Design Methodologies

The four design approaches outlined in this section and their design strengths compared to the actual tested values are summarized below in this section. Table 20 presents the design versus tested shear ratios for all of the methods, showing the overall correlation between the

Table 20: Comparison of Design Methods using Design Material Values

Shear Reinforcing	Maximum by Code				Full Strength				Failure
	AASHTO MCFT	ACI 318	ACI 440.4	ACI 440.1	AASHTO MCFT	ACI 318	ACI 440.4	ACI 440.1	
Min NEFMAC	2.77	2.83	3.50	1.85	1.69	2.09	2.09	1.44	Yes, Shear
Typ NEFMAC	2.71	2.34	3.31	1.73	1.31	1.51	1.51	1.16	Yes, Shear

design methods. The table shows that for both design by code strength and full strength, ACI 440.1 provides the best fit for Bulb-T beams reinforced with NEFMAC grid. This is mostly due to the use of the shear funnel approach described in section 2.3.4 of this thesis. This approach provides a more ideal area of concrete that is providing shear resistance in the design. This method can become tedious in design, so other methods should still be considered. AASHTO MCFT is another viable method. When utilizing the design strength limitations, this method is extremely conservative. However, if the method can be altered to allow the use of the full strength of the material, it will provide a safe and economical design. Due to the strict stress limitation of 0.002 times the modulus of elasticity, ACI 440.4 provides the most conservative design, resulting in an overly reinforced and uneconomical section. The ACI 318 full strength method provides a decent fit for NEFMAC grid strength, and could provide a relatively quick and efficient design check for safety.

Table 21 shows the same comparison of the shear calculation methods with the use of the actual tested material values of the concrete and longitudinal steel. This table provides a more exact design comparison in the ideal scenario of knowing the exact material properties used. The

general trend for these results correlate well with the results from Table 20. Overall, ACI 440.1 provides the most economical design for both design by code and design with full strength. When utilizing the design with the full strength of materials, AASHTO MCFT is the most viable option. This method is already implemented in the design of reinforced and prestressed beams. Even though ACI 440.1 provides a more exact prediction than AASHTO MCFT, the shear funnel approach may not be a viable option when prestressing is used.

Table 21: Comparison of Design Methods using Actual Material Values

Shear Reinforcing	Maximum by Code				Full Strength				Failure
	AASHTO MCFT	ACI 318	ACI 440.4	ACI 440.1	AASHTO MCFT	ACI 318	ACI 440.4	ACI 440.1	
Min NEFMAC	2.45	2.90	3.62	1.92	1.72	2.15	2.15	1.49	Yes, Shear
Typ NEFMAC	2.23	2.37	3.40	1.79	1.32	1.54	1.54	1.19	Yes, Shear

To provide a greater understanding of how these four design methods compare when CFRP grid is used as the transverse reinforcement, the results for NEFMAC grid from this thesis were combined with results for C-grid obtained from a previous study by Ward (2016). The comparison of design methods using design material values is shown in Table 22. The design methods provided similar trends for both NEFMAC grid and C-grid. ACI 440.1 provides the best estimate for shear capacity for both CFRP grids when using both design by code strength and full strength. When designed with code strength, the other three methods provide safe but much more uneconomical designs for all beam specimens. However, once the full strength was used in the designs, all of the methods provided more economical results while maintain a safe design. This further shows that the current stress limitations provide designs that are too conservative and somewhat uneconomical.

Table 22: NEFMAC and C-Grid Comparison of Design Methods using Design Values

Shear Reinforcing	Maximum by Code				Full Strength				Failure
	AASHTO MCFT	ACI 318	ACI 440.4	ACI 440.1	AASHTO MCFT	ACI 318	ACI 440.4	ACI 440.1	
Min C-Grid	2.35	2.63	2.73	1.68	1.57	1.67	1.67	1.32	Yes, Shear
C-Grid Zip Tied	2.18	2.74	2.89	1.51	1.22	1.40	1.40	1.09	Yes, Shear
C-Grid Spaced	2.30	2.89	3.05	1.59	1.29	1.48	1.48	1.15	Yes, Shear
Min NEFMAC	2.77	2.83	3.50	1.85	1.69	2.09	2.09	1.44	Yes, Shear
Typ NEFMAC	2.71	2.34	3.31	1.73	1.31	1.51	1.51	1.16	Yes, Shear
Average	2.46	2.68	3.10	1.67	1.42	1.63	1.63	1.23	

Table 23 shows the same comparison between NEFMAC grid and C-grid with the use of the actual tested material values. The general trend of results is similar to the results from the design material values comparison. Overall, ACI 440.1 was safe and the most economical design for both CFRP grids. However, when using the full strength of the grids, AASHTO MCFT also provided safe and economical designs. For both CFRP grids, AASHTO MCFT is the most viable design option due to it already being used in the design for reinforced and prestressed beams. However, the shear design ϕ-factor in AASHTO is 0.9. Since the failure of the NEFMAC grid results in a complete loss of load carrying capacity of the section and limited testing has been performed, a recommended is ϕ-factor to use is 0.75.

Table 23: NEFMAC and C-Grid Comparison of Design Methods using Actual Values

Shear Reinforcing	Maximum by Code				Full Strength				Failure
	AASHTO MCFT	ACI 318	ACI 440.4	ACI 440.1	AASHTO MCFT	ACI 318	ACI 440.4	ACI 440.1	
Min C-Grid	2.27	2.50	2.60	1.63	1.44	1.49	1.49	1.20	Yes, Shear
C-Grid Zip Tied	2.15	2.69	2.88	1.50	1.11	1.25	1.25	0.99	Yes, Shear
C-Grid Spaced	2.27	2.83	3.04	1.58	1.17	1.32	1.32	1.04	Yes, Shear
Min NEFMAC	2.45	2.90	3.62	1.92	1.72	2.15	2.15	1.49	Yes, Shear
Typ NEFMAC	2.23	2.37	3.40	1.79	1.32	1.54	1.54	1.19	Yes, Shear
Average	2.27	2.66	3.11	1.68	1.35	1.55	1.55	1.18	

6 – Parametric Study on Anchorage Zone Design with CFRP Grids

6.1 – Introduction

A concern for the long term durability of prestressed beams is the cracking that occurs in the end zones during detensioning. VDOT is interested in a completely steel free beam, and in order to do so the end region needs of a with CFRP reinforced beam should have sufficient crack control. Two parametric studies were completed in this section. The first was designing anchorage zones with CFRP grid as the sole transverse reinforcement. The second study used a combination of steel stirrups and CFRP grids as a way to reduce current beam-end congestion of reinforcement for beams that are not in areas susceptible to high corrosion. This study used strut-and-tie modeling to design the anchorage zone of prestressed beams. The CFRP grids that were used in this design are NEFMAC grid and C-grid. Three Pre-Cast Bulb-T (PCBT) beams were used in this study with three different spans and prestressed strand counts, resulting in nine anchorage zone designs for each parametric study. These three beam sizes were chosen because they are sizes that are most commonly used in the field. These beams and layouts are presented in Table 24.

Table 24: Parametric Study Beam Selection

Beam Type	Beam Spacing (ft)	Span Length (ft)	# of 1/2 in. Diameter Strands
PCBT-45A	6	40	16
PCBT-45B	7.5	65	20
PCBT-45C	9	60	16
PCBT-61A	6	90	22
PCBT-61B	7.5	80	26
PCBT-61C	9	80	26
PCBT-77A	6	75	20
PCBT-77B	7.5	100	26
PCBT-77C	9	90	24

6.2 – Parametric Study Assumptions

Many assumptions about material properties were made for the parametric study. These assumptions apply to all beam cases performed in the study. Similar to the AASHTO provisions on steel stirrups, the strength of CFRP grids are limited by a certain working stress. Based on AASHTO, steel stirrups are allowed a working stress of 20 ksi. However, based on recommendations provided by Crispino (2007), steel stirrups are limited to 18 ksi for normal weight concrete. This recommendation is to account for the corrosive environment that VDOT is interested in implementing these new designs. The working stresses for the CFRP grids were calculated based on equivalent crack widths at equal shear loading between beams reinforced with either steel stirrups and the two types of CFRP grids. Crack widths for steel and C-grid reinforced beams were obtained from Ward (2016). Crack widths for the NEFMAC grid reinforced beam were obtained from testing in this thesis presented in Section 5. For each shear loading, comparisons in crack widths were made between both steel and NEFMAC grid as well as steel and C-grid. Through this process, the percent difference in crack width between steel and the two CFRP grids were determined, as well as the average percent difference of the load range. A positive percent difference meant that the material prevented cracks from widening better than steel. The average percent difference was the factor that altered the working stress from 18 ksi to the respective working stress for the grid types. The crack widths were determined using best fit lines for the shear load versus crack width of the typical reinforcement tests. The results of this method are summarized in Table 25. Since NEFMAC grid was worse at preventing cracks than steel reinforcing, the working stress limit was reduced to 9 ksi. C-grid provided better crack control than steel reinforcing, so the working stress limit was increased to

28 ksi. The working stresses allowed and the resulting maximum tow strengths for the material in the anchorage zone design are presented in Table 26.

Table 25: Comparison of Crack Control

	Crack Width (in.)			% Difference	
Shear Load (kip)	Steel	C-Grid	NEFMAC	Steel - C-Grid	Steel - NEFMAC
13	0.0042	0.0014	0.0045	100%	-7%
15	0.0064	0.0032	0.0103	67%	-47%
17	0.0086	0.005	0.0161	53%	-61%
19	0.0108	0.0068	0.0219	45%	-68%
23	0.0152	0.0104	--	38%	--
25	0.0174	0.0122	--	35%	--
			Average:	56%	-46%

`

Table 26: Allowable Working Stresses and Maximum Tow Strengths

Material	Working Stress, σ_w (ksi)	Area Per Tow (in^2)	Strength Per Tow (kip)
Steel	18	Varies	Varies
C-Grid	28	0.00286	0.08008
NEFMAC	9	0.027	0.243

Normal weight concrete was used with a unit weight of 150 lb/ft^3. The compressive strength of concrete at release is 5,500 psi. Using these two assumptions, the modulus of elasticity of the concrete at transfer was computed using AASHTO LFRD equation 5.4.2.4-1, shown in Equation 17.

$$E_{ci} = 33w^{1.5}\sqrt{f_{ci}} \quad \text{(Eq 17)}$$

Where:

E_{ci} = Concrete modulus of elasticity at transfer (ksi)

w = Unit weight of concrete (lb/ft^3)

f_{ci} = Compressive strength of concrete at release (psi)

The ultimate strength of the prestressed steel was taken as 270 ksi, and 75 percent of this strength, 202.5 ksi, used for the initial stress at transfer. Harping points for draped strands are assumed at 40 and 60 percent of the beam length. For prestressing strands, the rows were filled from the bottom-up for straight strands, and top-down for harped strands. The top row of harped strands was at a height of 2 in. below the top of the beam. All holes for prestessed strands were on 2 in. center-to-center spacing. Lastly, there are no debonded strands used in this study.

6.3 – Parametric Study Strut-and-Tie Model

The strut-and-tie model that is used for the design of prestressed anchorage zones in this thesis was developed by Crispino (2007). Based on an in-depth study on PCBT beams, Crispino developed a simple, double-tie, strut-and-tie model. This strut-and-tie model is shown below in Figure 39. The findings of the PCBT study found that the required stirrup area within $h/4$ and between $h/4$ and $3h/4$ are very similar. With these findings, the tension ties T1 and T2 were set equal to each other. The compressive strut was placed at $3h/4$ from the beam end to provide similar results to other models (Crispino, 2007). Two prestressing forces are present in this model. P1 is the force produced by the straight strand prestessing, and P2 is the force produced by the harped strand prestressing.

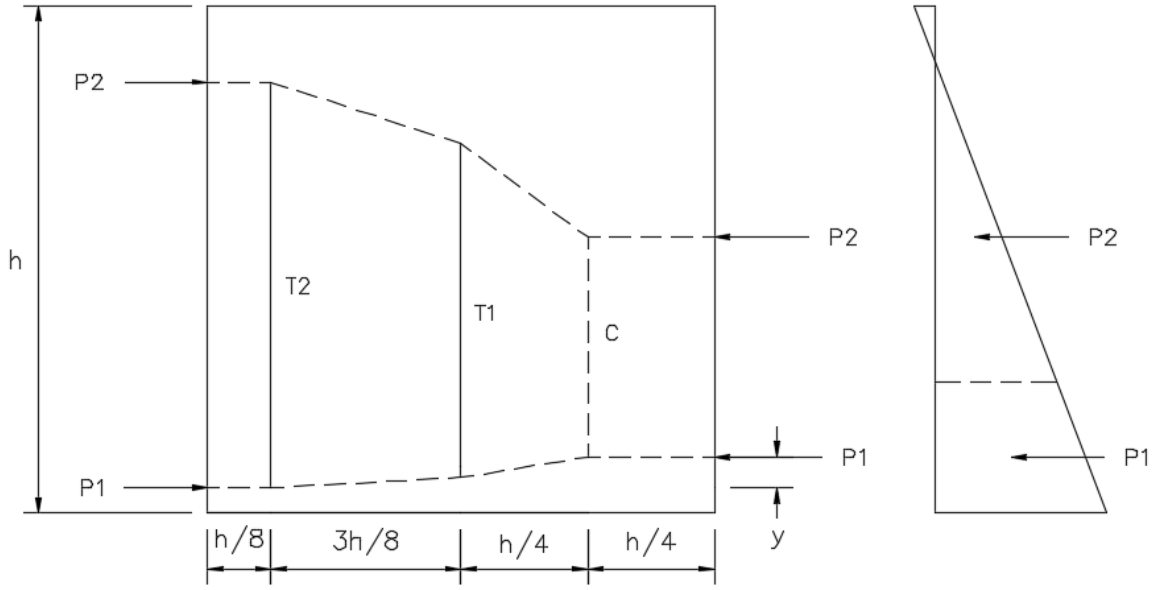

Figure 39: Strut-and-Tie Model

Crispino completed a symbolic derivation of this strut-and-tie model. By setting T1 and T2 equal, the derivation provided Equation 18.

$$T1 = T2 = \frac{8P_1 y}{7h} \quad \text{(Eq 18)}$$

Where:

P_1 = Force in straight strand group (kip)

y = difference in height between resultant force and applied prestress force (in.)

h = girder height (in.)

6.4 – Parametric Study Design Procedure

An excel spreadsheet was created to easily solve the strut-and-tie model above. The spreadsheet used the PCBT girder section properties, material properties of the concrete and

prestressed steel, and the strand pattern as input variables. After these initial constants were input, the spreadsheet calculated the transformed section properties at a distance h from the beam and at the harping point. Also, the tension and compression stresses were calculated at the top and bottom of these locations. The integration of the stress on the area of concrete from bottom-to-top was performed to determine the location of the resultant force. Once the location of the resultant force was determined, Equation 18 was used to determine the tension forces T1 and T2. With these tension forces calculated, the stirrup area within $h/4$ and between $h/4$ and $3h/4$ were calculated based on the working stresses for the material used. For the first parametric study, only CFRP grid was used as the stirrup reinforcement in the anchorage zone region. The second study combined CFRP grid with a pre-determined amount of steel stirrups for the design. The pre-determined amount of steel was determined based on ease of construction and reducing the amount of congestion in the reinforcement. Detailed examples of this procedure after finding the resultant force location are provided in the following two sections. See Appendix E for the process of completing the strut-and-tie model and calculating the resultant force location.

6.4.1 – Exclusively CFRP Grid End-Zone Design

In this section, an in-depth walkthrough of the calculations performed in the parametric study will be provided on the PCBT-45A girder section provided in Table 24. This design process was for the use of only CFRP grids as the transverse reinforcing in the anchorage zone region.

Based on the process shown in Appendix E, the values for the strut-and-tie model are calculated. The strut-and-tie model for this specific beam case is shown in Figure 40.

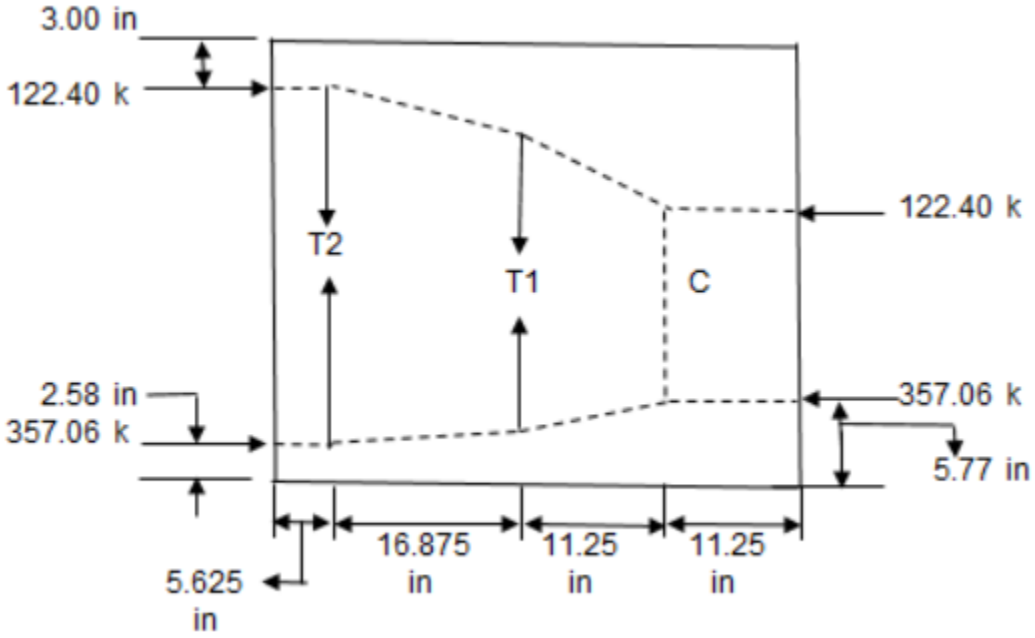

Figure 40: STM for PCBT-45A

Using this model and Equation 18, the tension ties, T1 and T2, are calculated as 28.9 kips each. This calculation is shown below:

$$T1 = T2 = \frac{8P_1 y}{7h}$$

$$T1 = T2 = \frac{8 * 357.06\ kip * (5.77\ in. - 2.58\ in.)}{7 * 45\ in.}$$

$$T1 = T2 = 28.9\ k$$

Once the tension ties are calculated, the length of the stirrup area within h/4 and between h/4 and 3h/4 were calculated as 11.25 in. and 22.5 in. respectively. With the known stirrup areas and vertical tow spacing for CFRP grids, the total number of vertical tows per layer within each stirrup area was calculated. Once the number of vertical tows per layer were calculated, the strength per layer of CFRP grid was calculated using the number of vertical tows and the

allowable strength per tow. Once these values were determined, the total number of layers of CFRP grid for each area was calculated.

A sample of this calculation is shown below for the T2 region using C-grid, with 1.6 in. tow spacing. The values for the sample calculations and the values for the other design cases of PCBT-45A are shown in Table 27.

$$\frac{h}{4} = \frac{45\ in.}{4} = 11.25\ in.$$

$$\frac{Vertical\ tows}{Layer} = 1 + \frac{stirrup\ area}{tow\ spacing} = 1 + \frac{11.25\ in.}{1.6\ in.}$$

$$\frac{Vertical\ tows}{Layer} = 8.03 = 8$$

$$\frac{Strength}{Layer} = \frac{Vertical\ tows}{Layer} * Allowable\ Tow\ Strength$$

$$\frac{Strength}{Layer} = 8 * 0.08008\ k = 0.641\ k$$

$$Minimum\ \#\ of\ Layers\ CFRP\ Grid\ Needed = \frac{T2}{Strength/_{Layer}}$$

$$Minimum\ \#\ of\ Layers\ CFRP\ Grid\ Needed = \frac{28.9\ k}{0.641\ k} = 45.1 = 46\ layers$$

Table 27: PCBT-45A – Exclusive CFRP Grid End-Zone Design

Tie	Required Strength (kip)	Distribution Length (in.)	Maximum Vertical Tows in Distribution Length per Layer of Grid		Strength Per Layer of Grid (kip)		Minimum # of CFRP Layers Needed	
			NEFMAC	C-Grid	NEFMAC	C-Grid	NEFMAC	C-Grid
T1	28.9	22.5	3	15	0.729	1.201	40	25
T2	28.9	11.25	2	8	0.486	0.641	60	46

As shown in Table 27, for the PCBT-45A example, the number of layers needed for each case is large. For the region of beam-end to $h/4$ (T2), NEFMAC grid and C-grid required 60 layers and 46 layers, respectively, to meet the strength requirements. For the region between $h/4$ and $3h/4$ (T1), NEFMAC grid and C-grid required 40 layers and 25 layers, respectively, to meet the strength requirements.

6.4.2 – Steel with CFRP Grid End-Zone Design

In this section, a second end-zone design case was used where single-legged steel stirrups were used in combination with CFRP grid. The design process is identical to the previous example until the calculations for the strength per layer of CFRP were made. For simplicity, the calculations used the same T2 region with C-grid reinforcing as the example in Section 6.4.1. This examples used the same PCBT-45A girder section provided in Table 24. The outlined example process in this section began after the calculation for the strength per layer of C-grid was completed.

The first step in this process was determining the steel stirrup layout that would help reduce congestion in the beam while providing the necessary reinforcing when combined with CFRP grid. The bars selected for the T2 region were 3 No. 5 bars spaced at 5 in. center-to-center. After this layout was selected, the total bar area was calculated. With the total bar area in the region, it was possible to determine how much of the force for T2 was reinforced through the steel. This was done by multiplying the allowable working stress for steel by the total bar area. Once this was determined, the remaining force of T2 that needed to be distributed to reinforcing was calculated. After this force was calculated, the total number of CFRP layers needed was calculated. The sample calculation for this design case is shown below, with the tabulated results for the other design cases shown in Table 28.

$$A_v = \#\ of\ bars * bar\ area$$

$$A_v = 3 * 0.31\ in.^2 = 0.93\ in.^2$$

$$T2_s = \sigma_W A_v$$

$$T2_s = 18\ ksi * 0.93\ in.^2 = 16.74\ k$$

$$T2_{CFRP} = T2 - T2_s$$

$$T2_{CFRP} = 28.9\ k - 16.74\ k = 12.16\ k$$

$$Minimum\ \#\ of\ Layers\ CFRP\ Grid\ Needed = \frac{T2_{CFRP}}{Strength/_{Layer}}$$

$$Minimum\ \#\ of\ Layers\ CFRP\ Grid\ Needed = \frac{12.16\ k}{0.641\ k} = 18.97 = 19\ layers$$

Table 28: PCBT-45A – Combined Steel and CFRP Grid End-Zone Design

Tie	Required Strength (kip)	Distribution Length (in.)	Steel Bar Size and Spacing	Total Steel Reinforcing, A_v ($in.^2$)	Strength from Steel, $T2_s$ (kip)	Minimum # of CFRP Layers Needed	
						NEFMAC	C-Grid
T1	28.9	22.5	4 #5 bars @ 8 in. spacing	1.24	22.32	9	6
T2	28.9	11.25	3 #5 bars @ 5in. spacing	0.93	16.74	25	19

As shown in Table 28, for this design case the number of layers remains high even with the steel reinforcing added. For the region of beam-end to h/4 (T2), 3 #5 bars were selected at 5 in. spacing. With this steel reinforcement, the beam end-zone needed 25 layers of NEFMAC grid and 19 layers of C-grid to meet strength requirements. For the region between h/4 and 3h/4 (T1), 4 #5 bars were selected at 8 in. spacing. With this steel reinforcement, the beam end-zone needed 9 layers of NEFMAC grid and 6 layers of C-grid to meet the strength requirements.

6.5 –Summary and Discussion of Parametric Study

For this study, 18 cases were performed for end-zone design. Nine consisted of using CFRP grid as the only type of transverse reinforcing, and the other nine consisted of using CFRP grid in addition to steel stirrup reinforcing. Table 29 shows a summary of all of these 18 designs. The table is split into two portions for design of the end-zones, using only CFRP grid as reinforcement and using a combination CFRP grid and steel reinforcement. The detailed tables shown in Sections 6.4.1 and 6.4.2 are shown in Appendix F for all of the design cases.

As shown in Table 29, the amount of CFRP grid layers needed for design are very high for both test methods. For the design utilizing only CFRP grid, the number of NEFMAC layers needed ranges from 36 to 100 layers. Even the smallest number of layers needed is far greater than is feasible to fit into the design. This is similar for C-grid, which ranges from 25 to 61 layers needed for design. As expected, when utilizing steel in combination with CFRP grid there was a decrease in the amount of CFRP grid layers needed for each design case. However, this decrease was not large enough to be implemented in real design and construction.

Based on these findings, CFRP grid is not a viable reinforcing material to be used in design for end-zone regions of prestressed beams. The stress limits placed on the CFRP grid for designing end-zones reduce the design strengths too much to design with properly. If VDOT wants to implement CFRP grids in design standards, then the current limits on working stresses for the CFRP grids need to be altered.

Table 29: End-Zone Design Summary for Both Methods

Beam	Tie Region	Exclusive CFRP Grid Reinforcement		Combined CFRP grid and Steel Reinforcement		
		Minimum # of CFRP grid Layers		Bar Size and Spacing	Minimum # of CFRP grid Layers	
		NEFMAC	C-Grid		NEFMAC	C-Grid
PCBT-45A	T1	40	25	4 #5 bars @ 8 in. spacing	9	6
	T2	60	46	3 #5 bars @ 5in. spacing	25	19
PCBT-45B	T1	49	30	4 #5 bars @ 8 in. spacing	18	11
	T2	73	55	3 #5 bars @ 5in. spacing	38	29
PCBT-45C	T1	46	28	4 #5 bars @ 8 in. spacing	15	9
	T2	68	52	3 #5 bars @ 5in. spacing	34	26
PCBT-61A	T1	44	27	5 #5 bars @ 7 in. spacing	15	10
	T2	88	53	3 #5 bars @ 7 in. spacing	53	33
PCBT-61B	T1	44	27	5 #5 bars @ 7 in. spacing	15	10
	T2	88	53	3 #5 bars @ 7 in. spacing	53	33
PCBT-61C	T1	50	31	5 #5 bars @ 7 in. spacing	21	13
	T2	100	61	3 #5 bars @ 7 in. spacing	65	40
PCBT-77A	T1	36	22	5 #5 bars @ 10 in. spacing	14	8
	T2	60	42	5 #5 bars @ 5 in. spacing	22	16
PCBT-77B	T1	45	28	5 #5 bars @ 10 in. spacing	22	14
	T2	75	53	5 #5 bars @ 5 in. spacing	37	26
PCBT-77C	T1	42	26	5 #5 bars @ 10 in. spacing	19	12
	T2	70	49	5 #5 bars @ 5 in. spacing	32	22

7 – Conclusions and Design Recommendations

7.1 – Proposed Design Methods

Based on the findings of the thesis the following proposed design and handling methods for shear design with NEFMAC grid are given below:

- Use manufacturer's reported strength and modulus of elasticity for NEFMAC grid
- Use the AASHTO Modified Compression Field Theory equation based format for shear calculations using manufacturer's data
- Use a minimum of 4 in. of development length with NEFMAC C6 for single layers of grid
- Recommended use of maximum 1/2 in. aggregate and 6-1/2 in. slump for concrete to allow proper consolidation of concrete

- Recommended ϕ-factor for shear as 0.75 due to limited testing and failure of NEFMAC grid as shear reinforcing results in a complete loss of section's load carrying capacity

For anchorage zone design, CFRP grids are not a viable option of reinforcement due to the current limitations set to reduce cracking. According to the NHRCP presented by Tadros et al. (2010), anchorage zone cracks do not negatively affect the structural integrity of beams. The main impact anchorage zone cracking causes is allowing corrosive agents to reach the prestressing steel in the beam. Since VDOT is interested in creating completely steel free bridge girders with CFRP, these corrosive agents would not have a great effect on the reinforcing. Therefore, when only CFRP reinforcing is used, the limitations on stress to reduce cracking within the anchorage zone should be removed. This will allow the full strength of CFRP reinforcing to be used in design.

7.2 – NEFMAC Grid Design Example

The design example comes from the PCI Bridge Design Manual Chapter 9, Section 9.4 (PCI Bridge Design Manual Steering Committee, 2003). The example is the Bulb-Tee (BT-72) Single Span, Composite Deck, LRFD Specifications example. This example provides guidance for the use of NEFMAC grid transverse reinforcement to ensure adequate shear capacity of the BT-72 beam. Layers of NEFMAC grid are staggered to create a vertical tow spacing of 5 in.

The bridge is a 120 ft span with no skew made up of BT-72 prestressed girders. The girders are spaced at 9 ft on center with an 8 in. uniform thickness composite deck above, including the 1/2 in. wearing surface. This provides a composite structural deck of 7-1/2 in. The design live load is specified as AASHTO HL-93. The design for flexure resulted in the use of 48 1/2 in. prestressing strands distributed in ten layers. The top 12 strands were harped in the section, with the harping occurring over the final 48 ft 6 in. of the beam.

Section 9.4.11 of the example provides the necessary information to perform the shear design. The critical shear depth, d_v, is 73.14 in. as shown in 9.4.11.1.3. Continuing through the calculations of the section shows an ultimate shear load, V_u, as 316.2 kips at the critical section as previously found in section 9.14.11.2.1. Calculation of the strain in the tensile steel led to the values of θ=22.8°, and β=2.94 as shown in 9.4.11.2.2. The shear resistance of the concrete, V_c, is 103.9 kips and the prestressing shear resistance, V_p, is 23.4 kips. Using the design equations and ϕ factor of 0.90 for normal weight concrete sections in shear, the shear resistance of the reinforcing, V_s, must be at least 188.9 kips. Due to the limited testing the ϕ-factor for shear is recommended to be used as 0.75. Therefore, the V_s required becomes 294.3 kips.

To provide this reinforcing the NEFMAC C6 grid is used. From the AASHTO method, the shear formula is given in this thesis as Equation 3. However, when using the equation, it is easy to modify to find the number of grids required as shown below.

$$n = \frac{V_s s}{F_{frp} d_v \cot\theta} \quad \text{(Eq 19)}$$

Where:

n = number of layers of grid needed

F_{frp} = Strength of grid provided by manufacturer (k)

The NEFMAC C6 has a 5 in. spacing in this design and F_{frp} is 4.69 kips/tow. From the example all other relevant variables to solve Equation 19 are given. Plugging in and solving provides a value for n as shown below in Equation 19.

$$n = \frac{294.3\ k * 5\ in.}{4.69\ k * 73.14\ in. * \cot(22.8°)} = 1.8 \quad \text{(Eq 20)}$$

Since 1.8 of staggered NEFMAC layers are needed, a total of four NEFMAC C6 layers are needed for the beam. Also, the grid meets all applicable spacing requirements of the beam

and minimum reinforcement areas of the beam. The next important step is to ensure the grid has enough embedment in the flange and bulb of the beam to develop full strength. The top flange of the beam provides 7-1/2 in. for development and the bulb provides 10-1/2 in. Since the NEFMAC grid can develop in 4 in., the beam provides adequate embedment for full development with room for clear cover. The four layers of NEFMAC grid will also fit easily into the 6 in. thick web with clear cover.

To summarize the design:

- Use four layers of NEFMAC C6 with grids staggered to create 5 in. spacing of vertical tows
- Provide 1 in. minimum spacing between layers in web
- Use one layer of NEFMAC grid on each side of prestressing strands to allow for ease of placement and spacing of grid
- Provide 1-1/2 in. clear cover at bottom
- Top will be covered with deck so cover not mandatory

7.2– Conclusions

The observed experimental results and comparison of the data to current codes, specifications, and design recommendations has led to the following conclusions for NEFMAC grid as shear reinforcing:

- NEFMAC is a viable shear reinforcement option for concrete bridge girders
- A single layer of NEFMAC C6 has a development length of 4 in.
- AASHTO modified compression field theory equations provide the best prediction of shear strength for NEFMAC grid when using the manufacturer's reported strength

- NEFMAC grid stress should not be reduced to code prescribed maximum or results will be overly conservative
- Use a shear design ϕ-factor of 0.75 due to limited amount of testing
- The manufacturer's reported strength can be used as long as it is reduced by three standard deviations
- Failure of beam with NEFMAC grid results in complete loss of load carrying capacity of section, as there is no additional yielding with CFRP materials

Based on current design specifications and limitations, CFRP grid is not a viable substitute for steel reinforcing in anchorage zone design of prestressed beams. The limitations in place to reduce anchorage zone cracking caused the design with CFRP grids to be overly conservative, resulting in designs that could not be implemented.

8 – Recommendations for Future Research

While this thesis provided some baseline recommendations on the use of CFRP transverse reinforcement, several areas could use further research. The following are suggestions for additional study:

- Full-scale prestress and reinforced beam tests with CFRP grid transverse reinforcement to ensure designs scale up properly and to ensure safe design recommendations.
- Full-scale prestress beam anchorage zone tests with CFRP grid transverse reinforcement to more effectively compare CFRP grid and steel stirrup reinforcing in this area.
- Testing to determine the required clear cover to fully develop NEFMAC grid to ensure a splitting failure of the concrete face does not occur.

- Testing to compare the bonded and non-bonded areas of NEFMAC grid and other CFRP grids to traditional steel reinforcing for similar design capacities.
- Testing to determine the viability of NEFMAC grid as horizontal shear reinforcement to provide adequate composite interaction between bridge deck and girders.
- Research to find CFRP materials for the use of confinement reinforcing in prestressed concrete beams.
- Development length testing for multiple layers of NEFMAC grid
- Additional testing with NEFMAC grid as shear reinforcement to help determine the reliability, properly calibrate the ϕ-factor, and to determine if a maximum allowable strain of NEFMAC is needed for a safe shear design.
- Changes to the AASHTO LFRD provisions for working stress limitations in anchorage zone reinforcement.

References

AASHTO (1998). *AASHTO LRFD Bridge Design Specifications, Second Edition with 2001 Interims*, American Association of State Highway and Transportation Officials, Washington, DC.

AASHTO. (2012). AASHTO LRFD bridge design specifications, 6th Ed., Washington, DC.

American Concrete Institute (ACI). (2004). "Prestressing concrete structures with FRP tendons." ACI 440.4R-04, Farmington Hills, MI.

American Concrete Institute (ACI). (2006). "Guide for the design and construction of structural concrete reinforced with FRP bars." ACI 440.1R-06, Farmington Hills, MI.

American Concrete Institute (ACI). (2014). "Building code requirements for structural concrete." ACI 318-14, Farmington Hills, MI.

ASTM C39/C39M-14a. (2014). Standard Test Method for Compressive Strength of Cylindrical Concrete Specimens. ASTM International, West Conshohocken, PA.

ASTM C469/C469M-14. (2014). Standard Test Method for Static Modulus of Elasticity and Poisson's Ratio of Concrete in Compression. ASTM International, West Conshohocken, PA.

ASTM C496/C496M-11. (2011). Standard Test Method for Splitting Tensile Strength of Cylindrical Concrete Specimens. ASTM International, West Conshohocken, PA.

Castrodale, R. W., Lui, A., and White, C. D., (2002). "Simplified Analysis of Web Splitting in Pretensioned Concrete Girders." *Proceedings, PCI/FHWA/NCBC Concrete Bridge Conference*, Nashville, TN, October 6-9.

Chomarat North America. (2010). Technical Data Sheet C50 1.8 x 1.6. Chomarat North America, Anderson, SC.

Chomarat North America. (2011). Test Method for Individual Strand Tensile Strength of C-Grid Products. Chomarat North America, Anderson, SC.

Crispino, E. D. (2007). *Anchorage zone design for pretensioned bulb-tee bridge girders in Virginia* (Thesis, Virginia Tech).

Ding, L., Rizkalla, S., Wu, G., & Wu, Z.S. (2011). Bond Mechanism of Carbon Fiber Reinforced Polymer Grid to Concrete (pp. 589-592). Berlin, Heidelberg: Springer Berlin Heidelberg.

Fam, A. Z. Y. H. (1996). Carbon fibre-reinforced plastic prestressing and shear reinforcements for concrete highway bridges. (Dissertation/Thesis), ProQuest, UMI Dissertations Publishing. Retrieved from http://vt.summon.serialssolutions.com/2.0.0/link/0/eLvHCXMwY2BQMLdMNTMyAR3snWqYkmhsapFsnmhokWiQlmKSmmoJvmgCseMdqTR3E2JgSs0TZZB1cw1x9tCFFY3xKTk58eYmoBlHUHdFjIE3EbT4O68EvEksRYJBwcLSIi3ZLCnNONU82SQlNTXJJDXF1DDNMMXU0iA1MdUEACoQJfw

Gergely, P. and Sozen, M. A. (1967). “Design of Anchorage Zone Reinforcement in Prestressed Concrete Beams,” *PCI Journal*, Vol. 12, No. 2, 63-75.

Grace, N. F., Jensen, E. A., Eamon, C. D., & Shi, X. W. (2012). Life-Cycle Cost Analysis of Carbon Fiber-Reinforced Polymer Reinforced Concrete Bridges. ACI STRUCTURAL JOURNAL, 109(5), 697-704.

Grace, N. F., Rout, S. K., Ushijima, K., & Bebawy, M. (2015). Performance of Carbon-Fiber-Reinforced Polymer Stirrups in Prestressed-Decked Bulb T-Beams. *JOURNAL OF COMPOSITES FOR CONSTRUCTION, 19*(3), 4014061. doi: 10.1061/(ASCE)CC.1943-5614.0000524

Grace, N. F., & Singh, S. B. (2003). Design approach for carbon fiber-reinforced polymer prestressed concrete bridge beams. ACI STRUCTURAL JOURNAL, 100(3), 365-376.

Grace, N., Ushijima, K., Baah, P., & Bebawy, M. (2013). Flexural Behavior of a Carbon Fiber–Reinforced Polymer Prestressed Decked Bulb T-Beam Bridge System. JOURNAL OF COMPOSITES FOR CONSTRUCTION, 17(4), 497-506. doi: 10.1061/(asce)cc.1943-5614.0000345

Jeong, S. K., Lee, S., Kim, C. H., Ok, D. M., & Yoon, S. J. (2006). Flexural behavior of GFRP reinforced concrete members with CFRP grid shear reinforcements. 306-308, 1361-1366.

Kannel, J., French, C., and Stolarski, H. (1997). “Release Methodology of Strands to Reduce End Cracking in Pretensioned Concrete Girders,” *PCI Journal*, Vol. 42, No. 1, 42-54.

Morphy, R., Shehata, E., & Rizkalla, S. (1997). Bent effect on strength of CFRP stirrups. Paper presented at the Proceedings of the Third International Symposium on Non-Metallic (FRP) Reinforcement for Concrete Structures.

Nabipaylashgari, M. (2012). Shear Strength of Concrete Beams Prestressed with CFRP Cables. (Dissertation/Thesis), ProQuest, UMI Dissertations Publishing. Retrieved from http://vt.summon.serialssolutions.com/2.0.0/link/0/eLvHCXMwY2BQSDQG9hLMk8yTk5JNU5KB7flE42TQoTBmFmlGlibgu1MQO96RSnM3IQam1DxRBjk31xBnD11Y0RifkpMTbwy6FdvQ0AzYXxFj4E0Erf7OKwHvEkuRYFAwtUwzN05OSzE1SUw0STI3TDIDNiRMUlOTkhKNLIFcADjJJW8

NEFMAC. (n.d.). Technical Data Sheet C6 8 x 10. NEFMAC, Japan.

Nislon, Arthur H. (1987). *Design of Prestressed Concrete*: *Second Edition.* Hoboken, NJ. Wiley.

PCI Bridge Design Manual Steering Committee. (2003). Precast Prestressed Concrete Bridge Design Manual.

Tadros, M.K., Badie, S.S., Tuan, C.Y. (2010). Evaluation and Repair Procedures for Precast/Prestressed Concrete Girders with Longitudinal Cracking in the Web. NCHRP Report 654. 16-32

Tureyen, A. K., Wolf, T. S., & Frosch, R. J. (2006). Shear strength of reinforced concrete T-beams without transverse reinforcement. ACI structural journal, 103(5).

Vecchio, F. J., & Collins, M. P. (1986). The modified compression-field theory for reinforced concrete elements subjected to shear. In ACI Journal Proceedings (Vol. 83, No. 2). ACI.

Ward III, J. C. (2016). *C-Grid as Shear Reinforcement in Concrete Bridge Girders* (Thesis, Virginia Tech).

Light, Strong, and Rust-Free NEFMAC ensures longer life for concrete structures.

Concrete bridge deck reinforced with carbon fibre **NEFMAC** grids

NEFMAC is an innovative concrete reinforcement consisting of high strength continuous fibres such as glass, carbon, and aramid, all of which are impregnated with resin and formed into a mesh.
NEFMAC is very light weight, stronger than steel reinforcement, free from rust and corrosion, and highly resistant to salt.
Patents have been applied for in eight countries.
(U.S.PAT. No. 4706430 and 4819395, Canadian PAT. No. 1278699, 1322217 and 2020436)

These are some of the many useful features of **NEFMAC**.

- *Rust-free and highly resistant to chemical agents*

Unlike steel reinforcing bars, **NEFMAC** is free from rust. Deterioration due to the harmful effects of salt water and chemical agents is minimized. This means **NEFMAC** ensures longer life for concrete structures.
Its non-magnetic property is another useful feature of **NEFMAC**.

- *Light weight and strong*

NEFMAC is light weight, stronger than steel reinforcement and easy to place. It improves on-site productivity and also reduces labour for transportation and placing.

- *Saves concrete*

The mesh crossing is in the same plane as reinforcing rods. Unlike steel bars, additional concrete cover is not needed to protect **NEFMAC**, and so **NEFMAC** can minimize cover thickness and save concrete.

- *Flexibility of Shapes*

NEFMAC is well suited to complex structures, such as curved surfaces, reinforcing of openings and three-dimensional structures.

■ Standard Specification of **NEFMAC**

TYPE	Bar No.	Sectional Area (in2)	* Max Load Kips	Tensile Strength (Ksi)	Modulus of Elasticity (Ksi)	Weight of Fiber (lbs/ft)
"G" GLASS FIBER	G2	0.007	0.58	86	4400	0.005
	G3	0.013	1.16			0.010
	G4	0.021	1.74			0.015
	G6	0.054	4.69			0.040
	G10	0.120	10.50			0.087
	G13	0.203	17.42			0.147
	G16	0.311	26.80			0.230
	G19	0.460	39.52			0.342
"C" CARBON FIBER	C6	0.027	4.69	173	14500	0.016
	C10	0.061	10.50			0.037
	C13	0.100	17.42			0.062
	C16	0.155	26.80			0.095
	C19	0.229	39.52			0.14
	C22	0.302	52.26			0.186
"A" ARAMID FIBER	A6	0.025	4.69	187	7800	0.014
	A10	0.056	10.50			0.031
	A13	0.093	17.42			0.051
	A16	0.143	26.80			0.079
	A19	0.210	39.52			0.117

* The maximum load for each type and size of 'NEFMAC' has been determined from short term tension tests, and is equal to the average tensile strength minus 3 x the standard deviation.

Applications of NEFMAC

NEFMAC has been successfully used as reinforcement to the following structures:

1. Concrete Bridge Decks.
2. Bridge barrier walls.
3. Tunnel linings. (shotcreting)
4. Precast wall claddings.
5. Slab-on-grade in highly corrosive environments.
6. Water inlet and outlet channels in power plant facilities.
7. Water and sewage storage tanks in treatment facilities.

Appendix B– Shear Test Calculations Example

AASHTO MCFT - Typical Reinforcement

Moment Capacity:

$$M_n = A_s f_y (d - \frac{a}{2})$$

$$A_s = \#\ of\ bars * bar\ area$$

$$A_s = 3 * 0.6\ in.^2 = 1.8\ in.^2$$

$$a = \frac{A_s f_y}{0.85 f'_c b}$$

$$a = \frac{1.8\ in.^2 * 60\ ksi}{0.85 * 7\ ksi * 16\ in} = 1.134\ in.$$

$$M_n = 1.8\ in.^2 * 60\ ksi((19\ in. - 2\ in.) - \frac{1.134\ in.}{2})$$

$$M_n = 148\ kip * ft$$

Shear Capacity:

$$V_n = V_s + V_c$$

$$V_s = \frac{A_v f_y d_v cot\theta}{s}$$

$$\theta = 29 + 3500\varepsilon_s$$

$$\theta = 29 + 3500 * 0.00215 = 36.5°$$

$$V_s = \frac{4.69\ k * 2\ layers * 16.43\ in. * \cot(36.5°)}{10\ in.}$$

$$V_s = 20.8\ k$$

$$V_c = 0.0316\beta\sqrt{f'_c} b_v d_v$$

$$\beta = \frac{4.8}{(1 + 750\epsilon_s)}$$

$$\beta = \frac{4.8}{(1 + 750 * 0.00215)} = 1.84$$

$$V_c = 0.0316 * 1.84\sqrt{7\ ksi} * 3\ in. * 16.43\ in.$$

$$V_c = 7.58\ k$$

$$V_n = 20.8\ k + 7.57\ k = 28.4\ k$$

Appendix C: Concrete Data

Data from cylinder testing of concrete used in development length and beam tests is presented below. Each entry is an individual cylinder that was tested.

Table 30: Complete Concrete Data for Tests

7 Day Tests		
Compression		
	4850	psi
	4770	psi
	5170	psi
14 Day Tests		
Compression		
	5930	psi
	5970	psi
	5890	psi
18 Day Tests		
Compression		
	6530	psi
	6210	psi
	6050	psi
Splitting Tensile		
	440	psi
	430	psi
Modulus of Elasticity		
	4560	ksi
	4510	ksi
19 Day Tests		
Compression		
	6680	psi
	6680	psi
	5890	psi
28 Day Tests		
Compression		
	7580	psi
	7360	psi
	7520	psi
Splitting Tensile		
	590	psi
	505	psi
	595	psi
Modulus of Elasticity		
	4820	ksi
	4980	ksi

Appendix D: Development Length Graphs

All load-displacement plots from the development length testing are shown below.

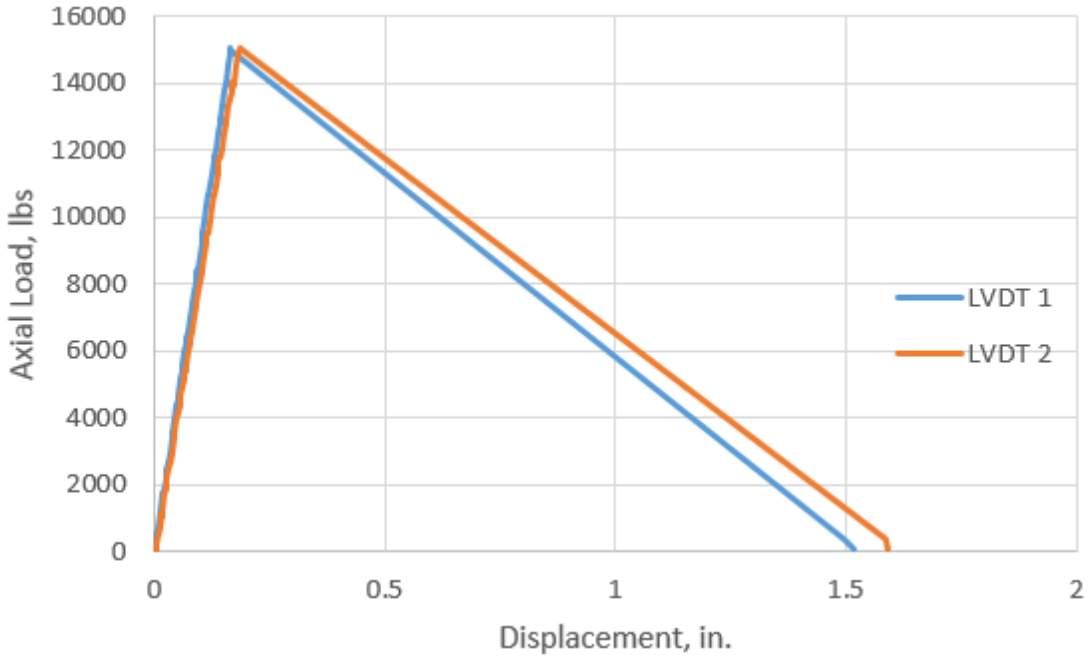

Figure 41: Development Length Load - Displacement Specimen 4-1

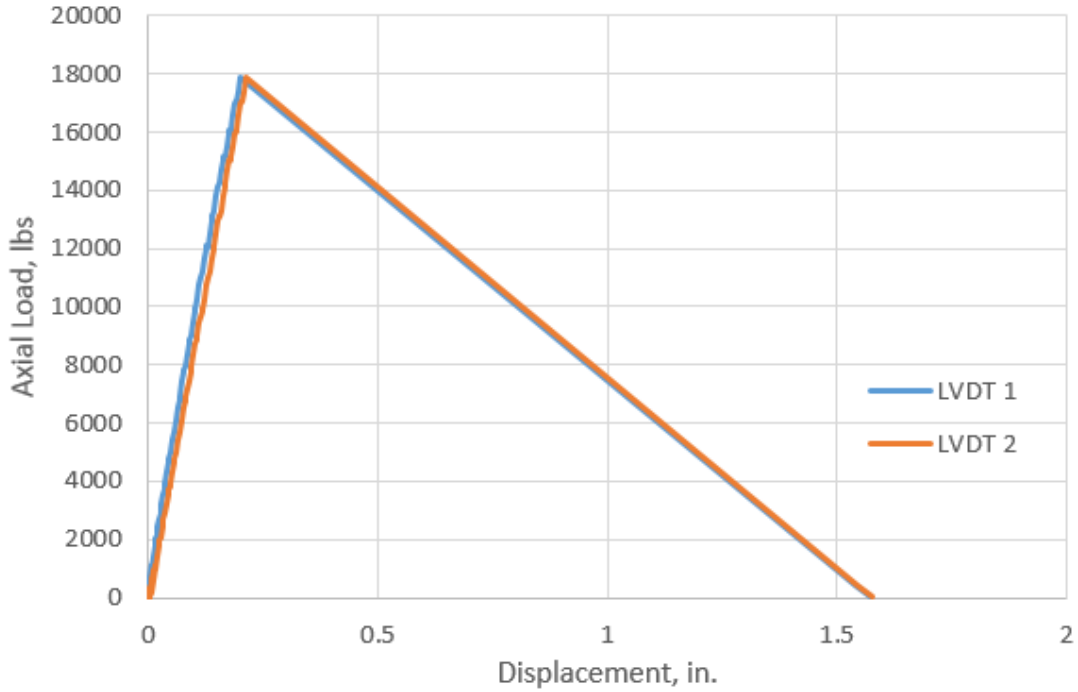

Figure 42: Development Length Load - Displacement Specimen 4-2

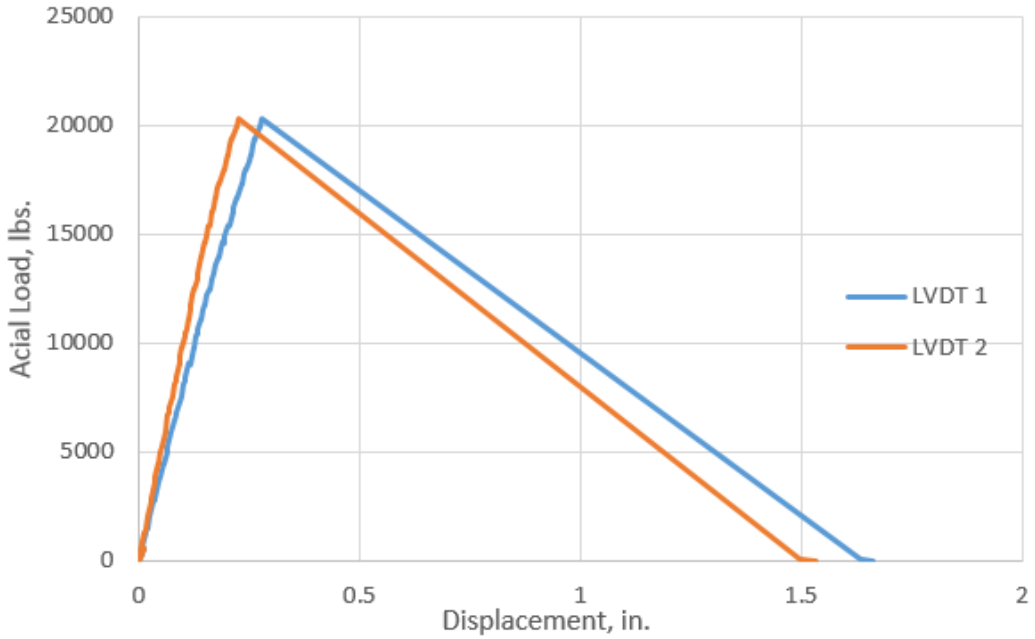

Figure 43: Development Length Load - Displacement Specimen 6-1

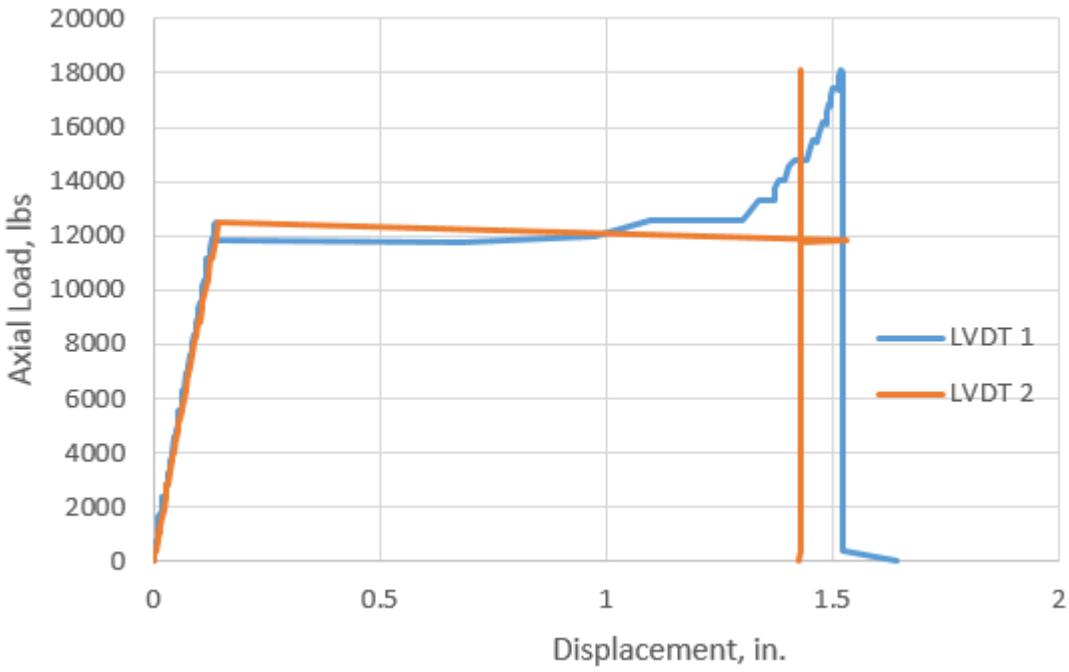

Figure 44: Development Length Load - Displacement Specimen 6-2

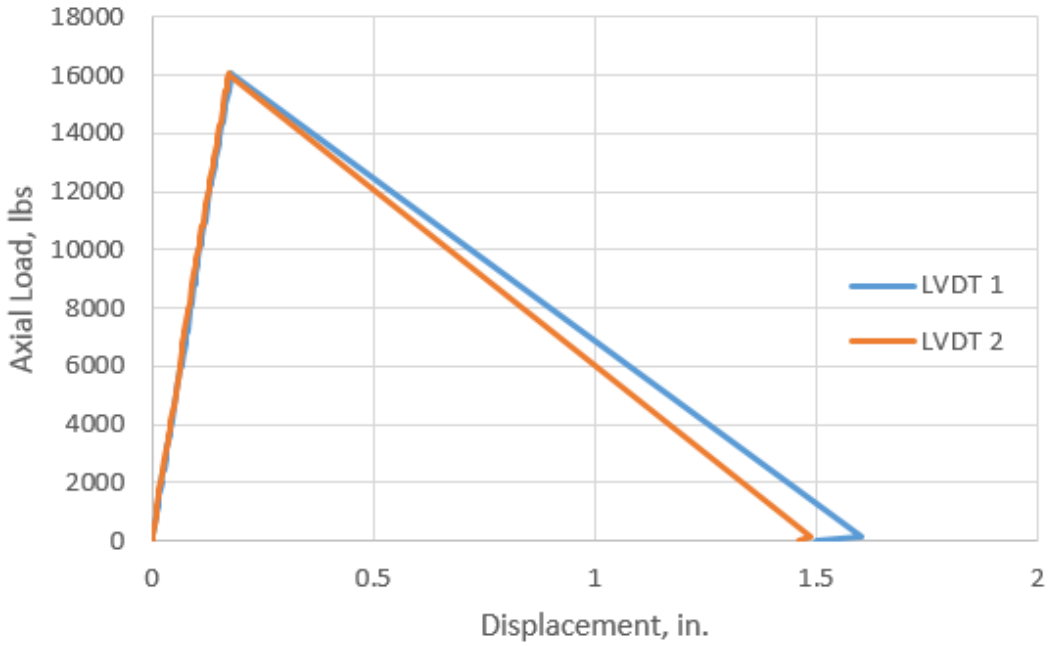

Figure 45: Development Length Load - Displacement Specimen 8-1

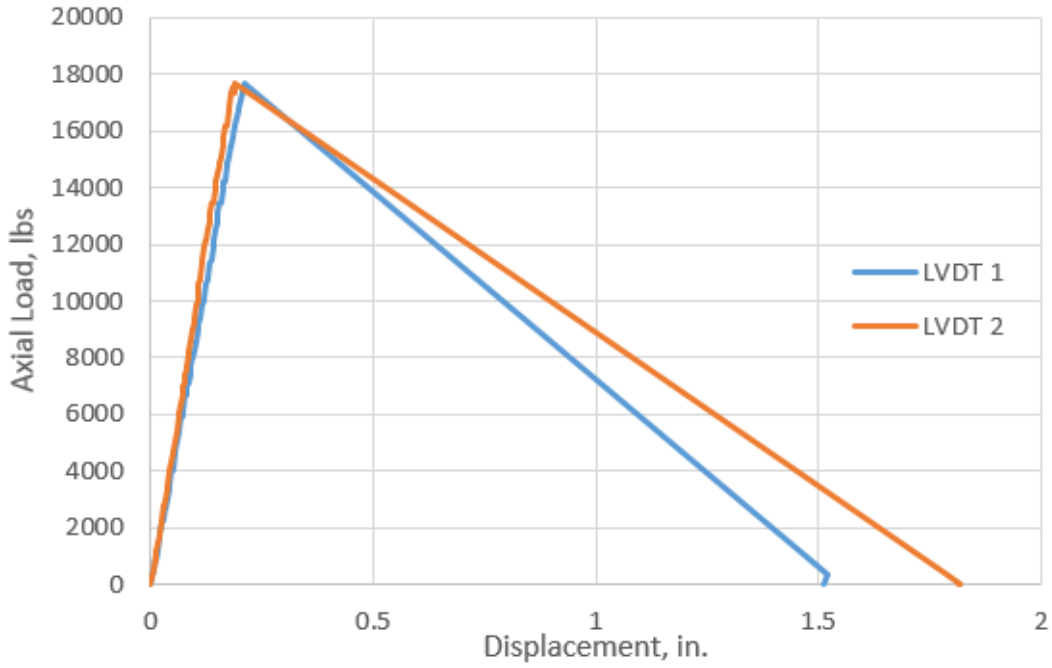

Figure 46: Development Length Load - Displacement Specimen 8-2

Appendix E: Design of Strut-and-Tie Model with PCBT-45A

This section outlines the design process used for creating the strut-and-tie model used in the parametric study.

Virginia PCBT-45A Bridge Girder Data

Depth of girder $h = 45\,in$

Area of girder $A_c = 746.7\,in^2$

Moment of inertia $I = 2.073 \times 10^5\,in^4$

Girder self-weight $w_o = 778\,\frac{lb}{ft}$

Girder Length $L = 40\,ft$

Height of centroid $y_b = 22.23\,in$

Strand Properties

$A_{strand} = 0.153\,in^2$

$f_{pu} = 270\,ksi$

$f_{jack} = 0.75 \cdot f_{pu}$

$E_{ps} = 28500\,ksi$

Concrete Material Properties

$\omega = 150\,pcf$

$f_{ci} = 5500\,psi$

$E_{ci} = 4227\,ksi$

Strand location at distance h from end of beam

Height of centroid of harped strands at beam end = 42 in.
Height of centroid of harped strands at harping point = 3.25 in.
Distance from end to harping point = 16 ft
Angle of harped strands, θ

$$\theta = \operatorname{atan}\left(\frac{42 - 3.25}{12 \cdot 16}\right) = 11.41\,\text{deg}$$

Height of centroid of harped stands at distance h from end of beam:

$$y_{cgs\_harped} = 42 - 45\tan(\theta) = 32.918$$

Height of centroid of straight strands at distance h from end of beam:

$$y_{cgs\_straight} = \frac{10(2.25) + 2(4.25)}{12} = 2.583 \quad \text{in.}$$

Properties of all prestressing steel at distance h from end of beam

	Area (in.^{2})	y_b (in.)	I (in.^{4})	P_{jack} (kips)
4 harped strands	0.612	32.9	4.126	124
12 straight strands	1.836	2.58	6.877	372
			Total =	496 kips

Transformed Section Properties at distance h from end of beam

Section modulus at transfer, n_i

$$n_i = \frac{E_{ps}}{E_{ci}} = 6.742$$

	n	A_T (in^2)	y_b (in)	$A_T y_b$ (in^3)	$A_T(y_b\text{-}y_T)^2$ (in^4)	I_o (in^4)	I^T (in^4)
Concrete		746.7	22.27	16629	37.37	207300	207337
Harped Strand	6.742	3.51	32.90	116	414.00	23.69	438
Straight Strand	6.742	10.54	2.58	27	3993.37	39.49	4033
	Total =	761	Total =	16772		Total =	211808

$$y_t = \frac{16772\text{in}^3}{761\text{in}^2} = 22.039\text{in} \text{ from bottom of beam}$$

Sample calculations for highlighted values

$$A_T = (n_i - 1)\cdot A_{ps\_harped} = 3.514\text{in}^2$$

$$I_o = (n_i - 1)\cdot I_{ps\_harped} = 23.693\text{in}^4$$

Stresses from prestress forces at distance h from end of beam

$$f_{bot} = \frac{P_{jack\_TOT}}{A_t} + \frac{y_t \cdot \left[P_{harped} \cdot \left(y_t - y_{b\_harped} \right) + P_{straight} \cdot \left(y_t - y_{b\_straight} \right) \right]}{I_t}$$

$$f_{bot} = -1.268\,ksi$$

$$f_{top} = \frac{P_{jack\_TOT}}{A_t} + \frac{\left(y_t - h \right) \cdot \left[P_{harped} \cdot \left(y_t - y_{b\_harped} \right) + P_{straight} \cdot \left(y_t - y_{b\_straight} \right) \right]}{I_t}$$

$$f_{top} = -0.0103\,ksi$$

Force in the strand groups after transfer

$$f_{cg\_straight} = 0.75 \cdot f_{pu} + n_i \cdot \left[f_{bot} + \frac{y_{b\_straight}}{h} \cdot \left(f_{top} - f_{bot} \right) \right]$$

$$f_{cg\_straight} = 194\,ksi$$

$$P_{straight} = f_{cg\_straight} \cdot 12 \cdot A_{strand} = 357\,kip$$

$$f_{cg\_harped} = 0.75 \cdot f_{pu} + n_i \cdot \left[f_{bot} + \frac{y_{b\_harped}}{h} \cdot \left(f_{top} - f_{bot} \right) \right]$$

$$f_{cg\_harped} = 200\,ksi$$

$$P_{harped} = f_{cg\_harped} \cdot 4 \cdot A_{strand} = 122\,kip$$

Integrate stress over concrete area from bottom of girder up until resultant force in concrete equals the applied force in the straight strand group strand group (357 kip)

Height (in)	Width (in)	Stress (ksi)	Force (k)	y_b (in)	TOT Force (k)	Force * y_b (in-k)
0	32	-1.146	0	0	0	0
7	32	-0.987	-238.9	3.413	-238.9	-815.3
10	14	-0.919	-65.8	8.482	-304.6	-557.8
13.5	7	-0.840	-32.3	11.724	-336.9	-378.9
17.1	7	-0.758	-20.1	15.269	-357.1	-307.5
					Σ =	-2059.466

Sample calculation for highlighted values

$$\text{Force} = \frac{(32+32)}{2}\cdot\frac{(-1.146-.987)}{2}\cdot(7-0) = -238.9 \text{ kip}$$

$$y_b = \frac{(7-0)[2(.987)+1.146]}{3\cdot(1.146+.987)} = 3.413 \text{ in.}$$

Find location of resultant force in concrete

$$y_{b\_resultant} = \frac{-2059.5\text{kip}\cdot\text{in}}{-357.1\text{kip}} = 5.767\text{in}$$

Solve Strut-and-Tie Model

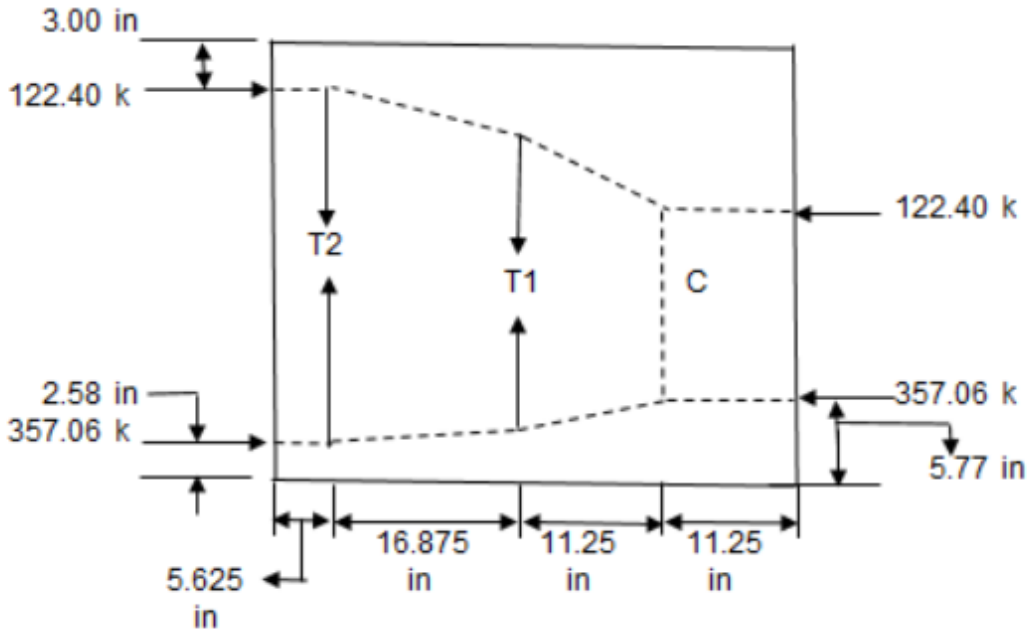

Calculate T1 and T2

$$T1 = \frac{8\cdot P_{straight}\cdot(y_{b\_resultant} - y_{cgs\_straight})}{7\cdot h} = 28.897\text{kip}$$

$$T1 = 28.897\text{kip}$$

$$T2 = T1$$

$$T2 = 28.897\text{kip}$$

Appendix F: Parametric Study Design Results

Table 31: PCBT-45A – Exclusive CFRP Grid End-Zone Design

Tie	Required Strength (kip)	Distribution Length (in.)	Maximum Vertical Tows in Distribution Length per Layer of Grid		Strength Per Layer of Grid (kip)		Minimum # of CFRP Layers Needed	
			NEFMAC	C-Grid	NEFMAC	C-Grid	NEFMAC	C-Grid
T1	28.9	22.5	3	15	0.729	1.201	40	25
T2	28.9	11.25	2	8	0.486	0.641	60	46

Table 32: PCBT-45B – Exclusive CFRP Grid End-Zone Design

Tie	Required Strength (kip)	Distribution Length (in.)	Maximum Vertical Tows in Distribution Length per Layer of Grid		Strength Per Layer of Grid (kip)		Minimum # of CFRP Layers Needed	
			NEFMAC	C-Grid	NEFMAC	C-Grid	NEFMAC	C-Grid
T1	35.1	22.5	3	15	0.729	1.201	49	30
T2	35.1	11.25	2	8	0.486	0.641	73	55

Table 33: PCBT-45C – Exclusive CFRP Grid End-Zone Design

Tie	Required Strength (kip)	Distribution Length (in.)	Maximum Vertical Tows in Distribution Length per Layer of Grid		Strength Per Layer of Grid (kip)		Minimum # of CFRP Layers Needed	
			NEFMAC	C-Grid	NEFMAC	C-Grid	NEFMAC	C-Grid
T1	32.8	22.5	3	15	0.729	1.201	46	28
T2	32.8	11.25	2	8	0.486	0.641	68	52

Table 34: PCBT-61A – Exclusive CFRP Grid End-Zone Design

Tie	Required Strength (kip)	Distribution Length (in.)	Maximum Vertical Tows in Distribution Length per Layer of Grid		Strength Per Layer of Grid (kip)		Minimum # of CFRP Layers Needed	
			NEFMAC	C-Grid	NEFMAC	C-Grid	NEFMAC	C-Grid
T1	42.4	30.5	4	20	0.972	1.602	44	27
T2	42.4	15.25	2	10	0.486	0.801	88	53

Table 35: PCBT-61B – Exclusive CFRP Grid End-Zone Design

Tie	Required Strength (kip)	Distribution Length (in.)	Maximum Vertical Tows in Distribution Length per Layer of Grid		Strength Per Layer of Grid (kip)		Minimum # of CFRP Layers Needed	
			NEFMAC	C-Grid	NEFMAC	C-Grid	NEFMAC	C-Grid
T1	42.4	30.5	4	20	0.972	1.602	44	27
T2	42.4	15.25	2	10	0.486	0.801	88	53

Table 36: PCBT-61C – Exclusive CFRP Grid End-Zone Design

Tie	Required Strength (kip)	Distribution Length (in.)	Maximum Vertical Tows in Distribution Length per Layer of Grid		Strength Per Layer of Grid (kip)		Minimum # of CFRP Layers Needed	
			NEFMAC	C-Grid	NEFMAC	C-Grid	NEFMAC	C-Grid
T1	48.2	30.5	4	20	0.972	1.602	50	31
T2	48.2	15.25	2	10	0.486	0.801	100	61

Table 37: PCBT-75A – Exclusive CFRP Grid End-Zone Design

Tie	Required Strength (kip)	Distribution Length (in.)	Maximum Vertical Tows in Distribution Length per Layer of Grid		Strength Per Layer of Grid (kip)		Minimum # of CFRP Layers Needed	
			NEFMAC	C-Grid	NEFMAC	C-Grid	NEFMAC	C-Grid
T1	43.7	38.5	5	25	1.215	2.002	36	22
T2	43.7	19.25	3	13	0.729	1.041	60	42

Table 38: PCBT-75B – Exclusive CFRP Grid End-Zone Design

Tie	Required Strength (kip)	Distribution Length (in.)	Maximum Vertical Tows in Distribution Length per Layer of Grid		Strength Per Layer of Grid (kip)		Minimum # of CFRP Layers Needed	
			NEFMAC	C-Grid	NEFMAC	C-Grid	NEFMAC	C-Grid
T1	54.3	38.5	5	25	1.215	2.002	45	28
T2	54.3	19.25	3	13	0.729	1.041	75	53

Table 39: PCBT-75C – Exclusive CFRP Grid End-Zone Design

Tie	Required Strength (kip)	Distribution Length (in.)	Maximum Vertical Tows in Distribution Length per Layer of Grid		Strength Per Layer of Grid (kip)		Minimum # of CFRP Layers Needed	
			NEFMAC	C-Grid	NEFMAC	C-Grid	NEFMAC	C-Grid
T1	50.8	38.5	5	25	1.215	2.002	42	26
T2	50.8	19.25	3	13	0.729	1.041	70	49

Table 40: PCBT-45A - Combined Steel and CFRP Grid End-Zone Design

Tie	Required Strength (kip)	Distribution Length (in.)	Steel Bar Size and Spacing	Total Steel Reinforcing, A_v (in.^{2})	Strength from Steel, $T2_s$ (kip)	Minimum # of CFRP Layers Needed	
						NEFMAC	C-Grid
T1	28.9	22.5	4 #5 bars @ 8 in. spacing	1.24	22.32	9	6
T2	28.9	11.25	3 #5 bars @ 5in. spacing	0.93	16.74	25	19

Table 41: PCBT-45B - Combined Steel and CFRP Grid End-Zone Design

Tie	Required Strength (kip)	Distribution Length (in.)	Steel Bar Size and Spacing	Total Steel Reinforcing, A_v (in.^{2})	Strength from Steel, $T2_s$ (kip)	Minimum # of CFRP Layers Needed	
						NEFMAC	C-Grid
T1	35.1	22.5	4 #5 bars @ 8 in. spacing	1.24	22.32	18	11
T2	35.1	11.25	3 #5 bars @ 5in. spacing	0.93	16.74	38	29

Table 42: PCBT-45C - Combined Steel and CFRP Grid End-Zone Design

Tie	Required Strength (kip)	Distribution Length (in.)	Steel Bar Size and Spacing	Total Steel Reinforcing, A_v (in.^{2})	Strength from Steel, $T2_s$ (kip)	Minimum # of CFRP Layers Needed	
						NEFMAC	C-Grid
T1	32.8	22.5	4 #5 bars @ 8 in. spacing	1.24	22.32	15	9
T2	32.8	11.25	3 #5 bars @ 5in. spacing	0.93	16.74	34	26

Table 43: PCBT-61A - Combined Steel and CFRP Grid End-Zone Design

Tie	Required Strength (kip)	Distribution Length (in.)	Steel Bar Size and Spacing	Total Steel Reinforcing, A_v (in.^{2})	Strength from Steel, $T2_s$ (kip)	Minimum # of CFRP Layers Needed	
						NEFMAC	C-Grid
T1	42.4	30.5	5 #5 bars @ 7 in. spacing	1.55	27.9	15	10
T2	42.4	15.25	3 #5 bars @ 7 in. spacing	0.93	16.74	53	33

Table 44: PCBT-61B - Combined Steel and CFRP Grid End-Zone Design

Tie	Required Strength (kip)	Distribution Length (in.)	Steel Bar Size and Spacing	Total Steel Reinforcing, A_v (in.^{2})	Strength from Steel, $T2_s$ (kip)	Minimum # of CFRP Layers Needed	
						NEFMAC	C-Grid
T1	42.4	30.5	5 #5 bars @ 7 in. spacing	1.55	27.9	15	10
T2	42.4	15.25	3 #5 bars @ 7 in. spacing	0.93	16.74	53	33

Table 45: PCBT-61C - Combined Steel and CFRP Grid End-Zone Design

Tie	Required Strength (kip)	Distribution Length (in.)	Steel Bar Size and Spacing	Total Steel Reinforcing, A_v (in.^{2})	Strength from Steel, $T2_s$ (kip)	Minimum # of CFRP Layers Needed	
						NEFMAC	C-Grid
T1	48.2	30.5	5 #5 bars @ 7 in. spacing	1.55	27.9	21	13
T2	48.2	15.25	3 #5 bars @ 7 in. spacing	0.93	16.74	65	40

Table 46: PCBT-75A - Combined Steel and CFRP Grid End-Zone Design

Tie	Required Strength (kip)	Distribution Length (in.)	Steel Bar Size and Spacing	Total Steel Reinforcing, A_v (in.^{2})	Strength from Steel, $T2_s$ (kip)	Minimum # of CFRP Layers Needed	
						NEFMAC	C-Grid
T1	43.7	38.5	5 #5 bars @ 10 in. spacing	1.55	27.9	14	8
T2	43.7	19.25	5 #5 bars @ 5 in. spacing	1.55	27.9	22	16

Table 47: PCBT-75B - Combined Steel and CFRP Grid End-Zone Design

Tie	Required Strength (kip)	Distribution Length (in.)	Steel Bar Size and Spacing	Total Steel Reinforcing, A_v (in.^{2})	Strength from Steel, $T2_s$ (kip)	Minimum # of CFRP Layers Needed	
						NEFMAC	C-Grid
T1	54.3	38.5	5 #5 bars @ 10 in. spacing	1.55	27.9	22	14
T2	54.3	19.25	5 #5 bars @ 5 in. spacing	1.55	27.9	37	26

Table 48: PCBT-75C - Combined Steel and CFRP Grid End-Zone Design

Tie	Required Strength (kip)	Distribution Length (in.)	Steel Bar Size and Spacing	Total Steel Reinforcing, A_v (in.^{2})	Strength from Steel, $T2_s$ (kip)	Minimum # of CFRP Layers Needed	
						NEFMAC	C-Grid
T1	50.8	38.5	5 #5 bars @ 10 in. spacing	1.55	27.9	19	12
T2	50.8	19.25	5 #5 bars @ 5 in. spacing	1.55	27.9	32	22